University of Reading

Impact of model resolution on tropical cyclone simulation using the HighResMIP–PRIMAVERA multimodel Ensemble

Article

Published Version

Roberts, M. J., Camp, J., Seddon, J., Vidale, P. L., Hodges, K., Vanniere, B. ORCID: https://orcid.org/0000-0001-8600-400X, Mecking, J., Haarsma, R., Bellucci, A., Scoccimarro, E., Caron, L.-P., Chauvin, F., Terray, L., Valcke, S., Moine, M.-P., Putrahasan, D., Roberts, C., Senan, R., Zarzycki, C. and Ullricu, P. (2020) Impact of model resolution on tropical cyclone simulation using the HighResMIP–PRIMAVERA multimodel Ensemble. Journal of Climate, 33 (7). pp. 2557-2583. ISSN 1520-0442 doi: https://doi.org/10.1175/JCLI-D-19-0639.1 Available at https://centaur.reading.ac.uk/92719/

It is advisable to refer to the publisher's version if you intend to cite from the work. See Guidance on citing.

Published version at: https://journals.ametsoc.org/jcli/article/33/7/2557/346417

To link to this article DOI: http://dx.doi.org/10.1175/JCLI-D-19-0639.1

Publisher: American Meteorological Society

All outputs in CentAUR are protected by Intellectual Property Rights law, including copyright law. Copyright and IPR is retained by the creators or other

University of Reading

copyright holders. Terms and conditions for use of this material are defined in the End User Agreement.

www.reading.ac.uk/centaur

CentAUR

Central Archive at the University of Reading

Reading's research outputs online

SPECIAL
U.S. CLIVAR Hurricanes
COLLECTION

Impact of Model Resolution on Tropical Cyclone Simulation Using the HighResMIP–PRIMAVERA Multimodel Ensemble

MALCOLM JOHN ROBERTS,[a] JOANNE CAMP,[a] JON SEDDON,[a] PIER LUIGI VIDALE,[b] KEVIN HODGES,[b] BENOIT VANNIERE,[b] JENNY MECKING,[c,m] REIN HAARSMA,[d] ALESSIO BELLUCCI,[e] ENRICO SCOCCIMARRO,[e] LOUIS-PHILIPPE CARON,[f] FABRICE CHAUVIN,[g] LAURENT TERRAY,[h] SOPHIE VALCKE,[h] MARIE-PIERRE MOINE,[h] DIAN PUTRASAHAN,[i] CHRISTOPHER ROBERTS,[j] RETISH SENAN,[j] COLIN ZARZYCKI,[k] AND PAUL ULLRICH[l]

[a] *Met Office, Exeter, United Kingdom*
[b] *National Centre for Atmospheric Science, University of Reading, Reading, United Kingdom*
[c] *University of Southampton, Southampton, United Kingdom*
[d] *Koninklijk Nederlands Meteorologisch Instituut, De Bilt, The Netherlands*
[e] *Fondazione Centro Euro-Mediterraneo sui Cambiamenti Climatici, Bologna, Italy*
[f] *Barcelona Supercomputing Center–Centro Nacional de Supercomputación, Barcelona, Spain*
[g] *Centre National de Recherches Météorologiques-Centre Europeen de Recherche et de Formation Avancee en Calcul Scientifique, Toulouse, France*
[h] *CECI, Université de Toulouse, CERFACS/CNRS, Toulouse, France*
[i] *Max Planck Gesellschaft zur Foerderung der Wissenschaften E.V. (MPI-M), Hamburg, Germany*
[j] *European Centre for Medium Range Weather Forecasting, Reading, United Kingdom*
[k] *The Pennsylvania State University, University Park, Pennsylvania*
[l] *University of California, Davis, Davis, California*

(Manuscript received 30 August 2019, in final form 28 December 2019)

ABSTRACT

A multimodel, multiresolution set of simulations over the period 1950–2014 using a common forcing protocol from CMIP6 HighResMIP have been completed by six modeling groups. Analysis of tropical cyclone performance using two different tracking algorithms suggests that enhanced resolution toward 25 km typically leads to more frequent and stronger tropical cyclones, together with improvements in spatial distribution and storm structure. Both of these factors reduce typical GCM biases seen at lower resolution. Using single ensemble members of each model, there is little evidence of systematic improvement in interannual variability in either storm frequency or accumulated cyclone energy as compared with observations when resolution is increased. Changes in the relationships between large-scale drivers of climate variability and tropical cyclone variability in the Atlantic Ocean are also not robust to model resolution. However, using a larger ensemble of simulations (of up to 14 members) with one model at different resolutions does show evidence of increased skill at higher resolution. The ensemble mean correlation of Atlantic interannual tropical cyclone variability increases from ~0.5 to ~0.65 when resolution increases from 250 to 100 km. In the northwestern Pacific Ocean the skill keeps increasing with 50-km resolution to 0.7. These calculations also suggest that more than six members are required to adequately distinguish the impact of resolution within the forced signal from the weather noise.

Denotes content that is immediately available upon publication as open access.

[m] Current affiliation: National Oceanography Centre, Southampton, United Kingdom.

Corresponding author: Malcolm John Roberts, malcolm.roberts@metoffice.gov.uk

DOI: 10.1175/JCLI-D-19-0639.1

© 2020 American Meteorological Society. For information regarding reuse of this content and general copyright information, consult the AMS Copyright Policy (www.ametsoc.org/PUBSReuseLicenses).

Downloaded from http://journals.ametsoc.org/jcli/article-pdf/33/7/2557/4930746/jclid190639.pdf by guest on 08 September 2020

1. Introduction

Tropical cyclone impacts globally are important for life and economies, being the largest driver of losses among natural hazards (Landsea 2000; Aon Benfield 2018). They also contribute significantly to regional seasonal rainfall totals (Jiang and Zipser 2010; Scoccimarro et al. 2014; Guo et al. 2017; Franco-Díaz et al. 2019) and hence form an important part of the mean climate. To achieve improved forecasts, risk assessment, and projections of future changes of tropical cyclones, better understanding of the drivers of interannual variability, and hence potential future changes in frequency or intensity, is key. Such understanding can only come from a combination of observations and modeling.

Previous assessments of tropical cyclone performance within global multimodel simulation comparisons have been hampered by a variety of factors (Camargo and Wing 2016). Use of models from the Coupled Model Intercomparison Projects (CMIP3 and CMIP5; Walsh et al. 2013; Camargo et al. 2013b) typically implies that model grid spacing is greatly restricted, typically to coarser than 100 km, and often considerably coarser, when effective resolution determined from the kinetic energy spectrum is considered (Klaver et al. 2019). This has consequences for both the model mean state and tropical cyclone characteristics. Specific projects such as the Tropical Cyclone-Model Intercomparison Project (TC-MIP; Walsh et al. 2010) and the U.S. Climate and Ocean: Variability, Predictability and Change (CLIVAR) Hurricane Working Group (Walsh et al. 2015) have investigated higher resolutions, but the simulations (and tracking algorithms) were not designed to be uniform and hence the results can be difficult to interpret (Camargo et al. 2013a; Shaevitz et al. 2014; Nakamura et al. 2017). There is also a need for multiple ensemble members so as to separate the forced signal from the weather noise (e.g., Zhao et al. 2009; Roberts et al. 2015; Mei et al. 2019).

There have also been many studies of the impact of horizontal resolution on tropical cyclones (Zhao et al. 2009; Manganello et al. 2012; Wehner et al. 2014; Kodama et al. 2015; Murakami et al. 2015; Roberts et al. 2015; Yoshida et al. 2017; Chauvin et al. 2019). These mainly used individual climate models, but due to differences in experimental design, tracking algorithm, model parameters, and other factors it can be difficult to understand how generally applicable the results are likely to be for other models.

The CMIP6 High Resolution Model Intercomparison Project (HighResMIP; Haarsma et al. 2016), in a new experimental design for CMIP6 (Eyring et al. 2016) that provides a common protocol for a multimodel, multiresolution ensemble. Some aspects of the simulation have been deliberately simplified (e.g., aerosol effects are imposed via specified optical properties) so that a comparison of model performance is made more manageable. This protocol extends the period of atmosphere-only simulations to 1950–2014 (as compared with the standard CMIP6 period of 1979–2014; Eyring et al. 2016) to assess a longer period of variability and drivers of change and increase the tropical cyclone (TC) sample sizes for climatology.

The European Union Horizon 2020 project PRIMAVERA (Process-based climate simulation: Advances in high-resolution modelling and European climate risk assessments; https://www.climateurope.eu/primavera/) has six different contributing global atmospheric models, each run using the HighResMIP protocol at both a standard CMIP6-type resolution (typically 100 km) and at a significantly higher resolution (toward 25 km), to investigate the impact this has on the simulation of climate variability and extremes, including tropical cyclones. It is a unique opportunity to understand the robustness of such changes across a range of models and resolutions. Two tracking algorithms—TRACK (Hodges et al. 2017) and TempestExtremes (Ullrich and Zarzycki 2017; Zarzycki and Ullrich 2017)—have been applied uniformly across all models and reanalyses to provide an indication in the uncertainties in the TC identification.

The key science questions addressed in this study are the following:

1) Are there robust impacts of higher resolution on explicit tropical cyclone simulation across the multimodel ensemble using different tracking algorithms?
2) What are the possible processes responsible for any changes with resolution?
3) How many ensemble members are needed to assess the skill in the interannual variability of tropical cyclones?

In section 2 we describe the models, forcing, and reanalysis datasets used in this study, together with the tracking algorithms and other datasets. In section 3 we describe our multimodel, multiresolution assessment of tropical cyclone performance, both as a global overview and then with focus on the North Atlantic Ocean. Here we also describe the impact of a larger ensemble size and the impact on skill for interannual variability. In section 4 we discuss the implications of our results and future work.

2. Model description, forcing, datasets, and tracking algorithms

Six PRIMAVERA modeling groups have configured global models at (at least) two horizontal resolutions

Downloaded from http://journals.ametsoc.org/jcli/article-pdf/33/7/2557/4930746/jclid190639.pdf by guest on 08 September 2020

and completed the Tier 1 CMIP6 HighResMIP atmosphere-only simulations (Haarsma et al. 2016) for 1950–2014. The models and resolutions are detailed in Table 1, including the ratio of the lower to higher grid spacing at the equator (Table 2). The effective resolution of the models (relating to the kinetic energy spectra) is described in Klaver et al. (2019) and is also included. Further HighResMIP experiments (Tier 2 coupled simulations and Tier 3 future projections) have also been completed, but the analysis of these is outside the scope of this work.

Detailed documentation on all models can be found in the following references, and is briefly summarized in appendix A: ECMWF-IFS (Roberts et al. 2018), CMCC-CM2 (Cherchi et al. 2019), CNRM-CM6 (Voldoire et al. 2019), MPI-ESM1.2 (Gutjahr et al. (2019), EC-Earth3P (Haarsma et al. 2019, manuscript submitted to *Geosci. Model Dev.*), and HadGEM3-GC3.1 (Roberts et al. 2019a). The HighResMIP protocol recommends minimal changes in model parameters between low- and high-resolution simulations in order that differences caused by resolution alone are emphasized. Table 3 describes all of the model parameters that are explicitly changed with resolution.

The inclusion of stochastic physics schemes, which attempt to represent the dynamical aspects of subgrid-scale processes, is becoming common for weather and seasonal forecasting (Palmer et al. 2009; MacLachlan et al. 2015; Walters et al. 2019), and is now being included in some global climate models (Batté and Doblas-Reyes 2015; Walters et al. 2019). Among the models used in this study, only the HadGEM3-GC3.1 and ECMWF-IFS contain such schemes. The influence of these schemes is designed to automatically decrease as model resolution becomes finer (i.e., by self-tuning rather than explicit parameter change; Sanchez et al. 2016) and hence needs to be considered when assessing "model resolution" impacts. Stochastic schemes have been shown to increase tropical cyclone mean frequency by up to 30% at some resolutions in multiple models (e.g., Met Office and ECMWF models; P. Vidale et al. 2019, unpublished manuscript), at least partly via moistening the tropical environment in the regions where the TCs have genesis (Watson et al. 2017).

All the models use an atmospheric initial condition at 1950 from the ECMWF reanalysis of the twentieth century (ERA-20C; Poli et al. 2016). Components of the land surface with longer memory (such as soil temperature and moisture) are initialized differently by each group; however, since the focus here is on the later 1979–2014 period of the simulations, this should have minimal impact on the results.

a. Forcing

The HighResMIP experimental design has been followed for the forcing datasets (Haarsma et al. 2016), including using simplified aerosol optical properties apart from one model (see below). These optical properties are a combination of a model constant background natural aerosol (typically diagnosed from a preindustrially forced simulation), together with time-varying volcanic and anthropogenic aerosol from the Max Planck Institute Aerosol Climatology, version 2 (MACv2-SP; Stevens et al. 2017), scheme. The latter uses sulfate aerosol patterns to scale the aerosol forcing magnitude over time. Note that this forcing by design excludes natural aerosol (including dust) variability and hence the simulations do not explicitly account for any variability driven by such forcing (Reed et al. 2019), apart from that which is integrated in the SST forcing itself. The exception to this is the CNRM-CM6.1 model, which uses its own aerosol scheme (Voldoire et al. 2019; Chauvin et al. 2019). A comparison of performance between MACv2-SP and prognostic aerosol is included in P. Vidale et al. (2019, unpublished manuscript).

The sea surface temperature (SST) and sea ice forcings used in the HighResMIP protocol are based on the daily, 1/4° Hadley Centre Global Sea Ice and Sea Surface Temperature (HadISST.2.2.0; Kennedy et al. 2017) dataset, with area-weighted regridding used to map this to each model grid. Mean differences between this dataset and the standard monthly Program for Climate Model Diagnosis and Intercomparison (PCMDI) SST used in the second Atmospheric Model Intercomparison Project (AMIP II; Taylor et al. 2000) are shown in P. Vidale et al. 2019, unpublished manuscript. The CMIP6 (Eyring et al. 2016) historic, time-varying forcings for solar (Matthes et al. 2017), ozone concentration (Hegglin et al. 2016), and greenhouse gases (GHG) (Meinshausen and Vogel 2016) are used. The land surface properties and land use remain constant, representative of the year 2000 using a repeating seasonal cycle.

b. Datasets

1) REANALYSES

The following reanalysis datasets are used: the European Centre for Medium-Range Weather Forecasts (ECMWF) interim reanalysis (ERA-Interim; Dee et al. 2011; 1979–2014); the fifth-generation ECMWF reanalysis (ERA5; Copernicus Climate Change Service 2017; 1979–2014); the NASA Modern-Era Retrospective Analysis for Research and Applications, version 2 (MERRA2; Gelaro et al. 2017; 1980–2014); the National Center for Atmospheric Research–Climate Forecast

Downloaded from http://journals.ametsoc.org/jcli/article-pdf/33/7/2557/4930746/jclid190639.pdf by guest on 08 September 2020

TABLE 1. Summary of models and their properties as used in PRIMAVERA project to complete the CMIP6 HighResMIP *highresSST-present* experiments. The expansions of most acronyms can be found online (https://www.ametsoc.org/PubsAcronymList). SISL = semi-implicit, semi-Lagrangian.

Institution	Met Office Hadley Centre; University of Reading; NERC	EC-Earth KNMI; Swedish Meteorological and Hydrological Institute; Barcelona Supercomputing Center; CNR	CERFACS	MPI-M	CMCC	ECMWF
Model name	HadGEM3-GC3.1	EC-Earth3P	CNRM-CM6.1	MPI-ESM1.2	CMCC-CM2-(V)HR4	ECMWF-IFS
Resolution names	LM, MM, HM	LR, HR	LR, HR	HR, XR	HR4, VHR4	LR, HR
Model atmosphere	MetUM	IFS cyc36r4	ARPEGE6.3	ECHAM6.3	CAM4	IFS cyc43r1
Atmospheric dynamical scheme (grid)	Grid point (SISL; lat–lon)	Spectral (linear; reduced Gaussian)	Spectral (linear; reduced Gaussian)	Spectral (triangular; Gaussian)	Grid point (finite volume; lat–lon)	Spectral (cubic octahedral; reduced Gaussian)
Atmospheric grid name	N96; N216; N512	Tl255; Tl511	Tl127; Tl359	T127; T255	1° × 1°; 0.25° × 0.25°	Tco199; Tco399
Atmospheric mesh spacing (0°N; km)	208; 93; 39	78; 39	156; 55	100; 52	100; 28	50; 25
Atmospheric mesh spacing (50°N; km)	135; 60; 25	71; 36	142; 50	67; 34	64; 18	50; 25
Atmospheric nominal res (CMIP6)	250; 100; 50	100; 50	250; 50	100; 50	100; 25	50; 25
Atmospheric model levels (top)	85 (85 km)	91 (0.01 hPa)	91 (78.4 km)	95 (0.01 hPa)	26 (2 hPa)	91 (0.01 hPa)

Downloaded from http://journals.ametsoc.org/jcli/article-pdf/33/7/2557/4930746/jcli190639.pdf by guest on 08 September 2020

TABLE 2. Information about model resolutions as used in this study. The effective resolution is taken from Klaver et al. (2019) and derived from examining model kinetic energy spectra, as is the "Lbox" value (calculated as a weighted grid box distance). The ratio of the low and high model resolution is calculated from both Lbox and the effective resolution (Eff resol). The analysis grid is the grid of the data as published on ESGF and as used for this analysis.

Model	HadGEM3-GC3.1	EC-Earth3P	CNRM-CM6.1	MPI-ESM1.2	CMCC-CM2-(V)HR4	ECMWF-IFS
LR-MR- HR	LM; (MM); HM	LR; HR	LR; HR	HR; XR	HR4; VHR4	LR; HR
Lbox	217; (96.7); 40.8	107; 54.2	207; 75.3	134; 66.9	153; 38.2	123; 62.8
Effective resolution [LR; (MR); HR]	590; (330); 135	375; 165	625; 230	605; 190	490; 150	290; 125
Resolution ratio (low/high) using Lbox (Eff resol)	5.32 (4.37)	1.98 (2.2)	2.75 (2.71)	2.0 (3.18)	4.0 (3.2)	1.95 (2.32)
Analysis grid	Native	Regridded 0.7 × 0.7; 0.35 × 0.35	Regridded 1.4 × 1.4;0.5 × 0.5	Native	Native	Regridded 1 × 1; 0.5 × 0.5

System Reanalysis (NCAR-CFSR; Saha et al. 2014; 1979–2014); and the Japanese 55-Year Reanalysis (JRA-55; Kobayashi et al. 2015; 1959–2014). An overview of the properties of these reanalysis datasets is given in Table 4. Tropical cyclones in these datasets (apart from ERA5) have been compared in Hodges et al. (2017) and Murakami (2014).

2) OBSERVATIONS

Observed tropical cyclone tracks for the North Atlantic and eastern Pacific Ocean basins are obtained from the National Oceanic and Atmospheric Administration (NOAA) National Hurricane Center's best-track Hurricane Database [HURDAT2 (January 2018 version); Landsea and Franklin 2013]. Observed tropical cyclone data for all remaining basins are obtained from the U.S. Navy's Joint Typhoon Warning Center (JTWC) best-track database (Chu et al. 2002). We define an observed tropical cyclone as having a 1-min maximum sustained wind speed of 34 kt (17.5 m s^{-1}) or higher, to give a globally uniform criterion, and we exclude subtropical storms (SS) from observations when they have SS as their officially designated maximum classification. We use these datasets in preference to IBTrACS (Knapp et al. 2010) for the consistency of 1-min averaging periods for all TCs around the world.

3) MODELS

Model simulation output can be obtained via the Earth System Grid Federation (ESGF) nodes from the following: Roberts (2017a,b,c; HadGEM3-GC3.1), Roberts et al. (2017a,b; ECMWF-IFS), Voldoire (2017, 2018; CNRM-CM6.1), Scoccimarro et al. (2017a,b; CMCC-CM2-(V)HR4), EC-Earth (2018a,b; EC-Earth3P), and von Storch et al. (2017a,b; MPI-ESM1.2). The storm tracks derived from these datasets and analyzed here are available from Roberts (2019a,b).

c. *Analysis information*

The analysis presented here focuses on the 1979–2014 period due to both the satellite observations providing a more homogeneous observational reference dataset, and the availability of multiple reanalysis datasets for validation.

The accumulated cyclone energy (ACE) index (Bell et al. 2000) is an integrated measure of tropical cyclone activity, and is calculated for model and observed tropical cyclones using the same method as Camp et al. (2015). For observed tropical cyclones, ACE is the sum of the square of the maximum sustained 10 m wind speed every 6 h while the cyclone is at least tropical storm strength (34 kt; 17.5 m s^{-1}). For model and reanalysis tropical cyclones, the wind speeds are lower than observed

TABLE 3. Summary of parameter differences between horizontal resolutions of the PRIMAVERA models used in HighResMIP *highresSST-present* simulations.

Model	Time step (min)	Parameter changes (reason)	Parameter values by resolution (from low to high)
HadGEM3-GC3.1 (LM; MM; HM)	20; 15; 10	Ultra-simple spectral parameterization launch factor (QBO period)	1.3; (1.2); 1.2
EC-Earth3P (LR; HR)	45; 15	No changes	
CNRM-CM6.1 (LR; HR)	15; 15	No changes	
MPI-ESM1.2 (HR; XR)	3.3; 1.5	Horizontal diffusion damping term (stability)	1.5; 0.5
CMCC-CM2 (HR4; VHR4)	30; 15	No changes	
ECMWF-IFS (LR; HR)	30; 20	Autoconversion threshold for rain over ocean RCLCRIT_SEA (net surface energy balance)	2.5×10^{-4}; 2.0×10^{-4}

Downloaded from http://journals.ametsoc.org/jcli/article-pdf/33/7/2557/4930746/jclid190639.pdf by guest on 08 September 2020

TABLE 4. Properties of the reanalysis datasets used in this study. Abbreviations: 4D-Var is 4D variational data assimilation; 3D-Var is 3D variational data assimilation; TL255 is triangular truncation 255, with linear grid (approximate horizontal grid spacing in parentheses); L60 is 60 vertical levels; GSI is gridpoint statistical interpolation; IAU is incremental analysis update. Analysis grid is the grid on which the tracking is performed.

Reanalysis	ERA-Interim	MERRA2	JRA-55	NCEP-CFSR	ERA5
Model grid (resolution)	TL255 (80 km)	Cubed sphere (50 km)	TL319 (55 km)	T382 (38 km)	TL1279 (31 km)
Assimilation	4D-Var	3D-Var GSI + IAU	4D-Var	3D-Var GSI	4D-Var
Atmospheric model levels (top)	L60 (0.1 hPa)	L72 (0.01 hPa)	L60 (0.1 hPa)	L64 (0.26 hPa)	L137 (0.01 hPa)
Analysis grid	480 × 241	576 × 361	288 × 145	720 × 361	1440 × 720

(Williams et al. 2015), and therefore the wind speed threshold is removed entirely, and instead we calculate ACE throughout the lifetime of the storm during its warm core phase using winds at 925 hPa to better compare the seasonal cycle and interannual variability with observations (henceforth ACE_{925}), as in Camp et al. (2015). The ACE metric has been found to be a more robust measure for interannual variability than simple storm counts (e.g., Villarini and Vecchi 2013; Scoccimarro et al. 2018), partly because it may reduce the impact of observational methods and short-lived storms (Landsea et al. 2010).

In general, models at the resolutions shown here are not able to represent very intense wind speeds [see Davis (2018) for theoretical/numerical limits], but are more able to generate strong minima in surface pressure (Manganello et al. 2012). Hence in order to better stratify the model storms by intensity, we use a surface pressure scale for the model intensity, rather than wind speed (Caron and Jones 2012; Roberts et al. 2015). The categories are defined in Table 5.

d. Tracking algorithms (trackers)

The tropical cyclones are diagnosed from models and reanalyses using two feature-tracking algorithms (henceforth trackers): TRACK (Hodges et al. 2017) and TempestExtremes (Ullrich and Zarzycki 2017; Zarzycki and Ullrich 2017). These are described in detail in appendix B and are briefly summarized here. TRACK is based on tracking vorticity features on a common T63 spectral grid with criteria for warm-core and lifetime. TempestExtremes tracks features using sea level pressure on the model grid, with criteria for warm-core and lifetime. Models and reanalyses are all tracked in the same way with the same parameters—for both trackers, the parameter choices are primarily derived from comparing tracked reanalysis datasets and observations (Hodges et al. 2017; Zarzycki and Ullrich 2017), although with differing emphasis (appendix B). One notable difference between the application of the trackers is the dependence on the model grid: TRACK transforms each model output to a common T63 grid for tracking, while TempestExtremes operates on the native model grid. No wind speed thresholds are applied to either tracker. A more detailed comparison between several trackers to better understand the cause of the differences, including using application of classification schemes to the systems (McTaggart-Cowan et al. 2013; Yanase et al. 2014), is ongoing (M. Roberts et al. 2019, unpublished manuscript).

We chose to use two trackers so as to obtain complementary viewpoints of model performance. We expect results to depend on the details of each tracker's criteria, as is found in other feature-tracking comparisons, for example Horn et al. (2014) for TCs, Neu et al. (2013) for extratropical cyclones, and Shields et al. (2018) for atmospheric rivers. In cases for which both trackers broadly agree, we can be more confident that our conclusions are not dependent on tracker details.

3. Results

a. Global TC activity and track density

Realistic simulation of the frequency and spatial distribution of tracks of tropical cyclones is an important prerequisite for understanding the risk of landfall and climate impacts, as well as for potential changes in regional mean precipitation.

A simple initial assessment of TC frequency from models, reanalyses, and observations is shown in Figs. 1 and 2, illustrating the total number of storms in the Northern and Southern Hemispheres (NH and SH, respectively) and the distribution in each NH ocean basin. It is informative to show this using two different trackers since there are several aspects that might be misinterpreted

TABLE 5. The storm intensity categories (CatPx) as measured by MSLP ranges as used in this work, together with the official Saffir–Simpson 1-min sustained wind speed classification.

Category (CatPx)	MSLP range	Official intensity using 1-min sustained wind speed ($m\,s^{-1}$)
0	≥994	18–32
1	$980 \le x < 994$	33–42
2	$965 \le x < 980$	43–49
3	$945 \le x < 965$	50–58
4	$920 \le x < 945$	58–70
5	$860 \le x < 920$	>70

Downloaded from http://journals.ametsoc.org/jcli/article-pdf/33/7/2557/4930746/jclid190639.pdf by guest on 08 September 2020

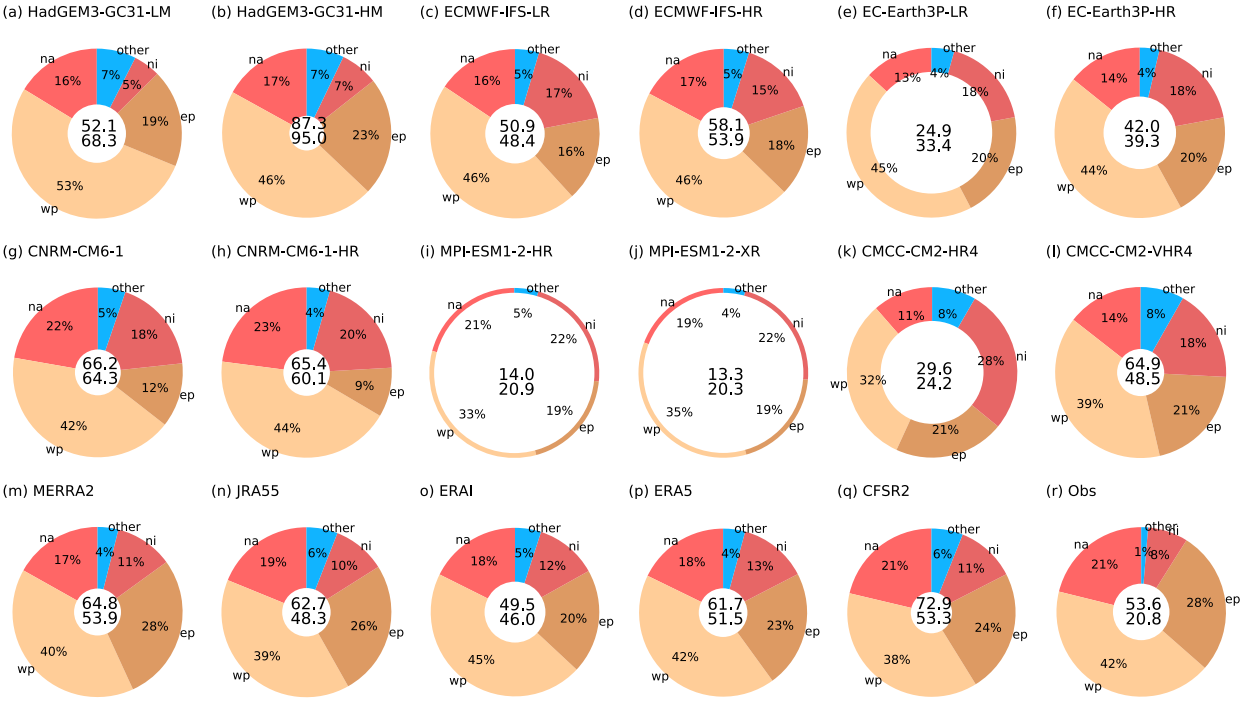

FIG. 1. Northern Hemisphere tropical cyclone frequency (mean storms per year during May–November, 1979–2014) from models, reanalyses, and observations, as diagnosed using the TRACK algorithm. The doughnut chart is divided into NH ocean basins; the totals in the center are (NH on top; SH underneath) mean storms per year (the Southern Hemisphere uses the October–May period). The thickness of the doughnut is scaled to the total NH TC observed frequency [i.e., doughnuts thicker than in (r) indicate more NH TCs, and thinner than in (r) indicate fewer NH TCs].

when just a single tracker is used. With TRACK (Fig. 1) there is a distinct increase in TC frequency with resolution for HadGEM3-GC31, CMCC-CM2-(V)HR4, and EC-Earth3P models, while all models and reanalyses typically have a smaller asymmetry of NH:SH TCs than is seen in the observations. The proportions of storms in each ocean basin agree reasonably well with observations, although for most models the relative frequency in the North Atlantic is less than observed while in the north Indian Ocean it is more. The overall NH TC frequency for the high-resolution models typically approaches or exceeds that observed.

Using TempestExtremes (Fig. 2) a somewhat different picture emerges compared to the above. Now there are only two models (HadGEM3-GC3.1 and CNRM-CM6.1) that have NH frequencies approaching or exceeding the observed. There is now a more systematic increase in TC frequency with resolution, and the hemispheric asymmetry is more consistent with that observed.

Several conclusions can be drawn from this simple comparison of models and trackers. Great care is needed when interpreting absolute TC frequency from a single tracker, since this will depend on many factors, including the tracker criteria and analysis grid. Features such as the hemispheric asymmetry could lead to the conclusion that the models produce too many SH TCs, but at least in part this seems to depend on how such storms are initially characterized (by vorticity or sea level pressure); observational issues could also contribute to the difference between models and observations, for example because SH tropical depressions and subtropical cyclones are not included in best-track data whereas they are in the NH (Strachan et al. 2013; Hodges et al. 2017).

Evaluation of the models' ability to simulate the spatial distribution of tropical cyclone tracks globally is shown in Fig. 3. This shows track density derived from TRACK and observations, defined by the mean number of tracks per month through a 4° cap at each point during May–November in the NH and November–May in the SH on a common grid. For each pair of plots, the bias in the higher-resolution model is shown first, followed by the difference between the higher- and lower-resolution model.

Key aspects include the following:

- Most models show a reduction in the negative density bias in the North Atlantic and the northwestern and eastern Pacific when resolution is increased.
- Many models have an excess of activity in the Southern Hemisphere, including in the South Atlantic, which is enhanced at higher resolution, as discussed above.

Downloaded from http://journals.ametsoc.org/jcli/article-pdf/33/7/2557/4930746/jcli190639.pdf by guest on 08 September 2020

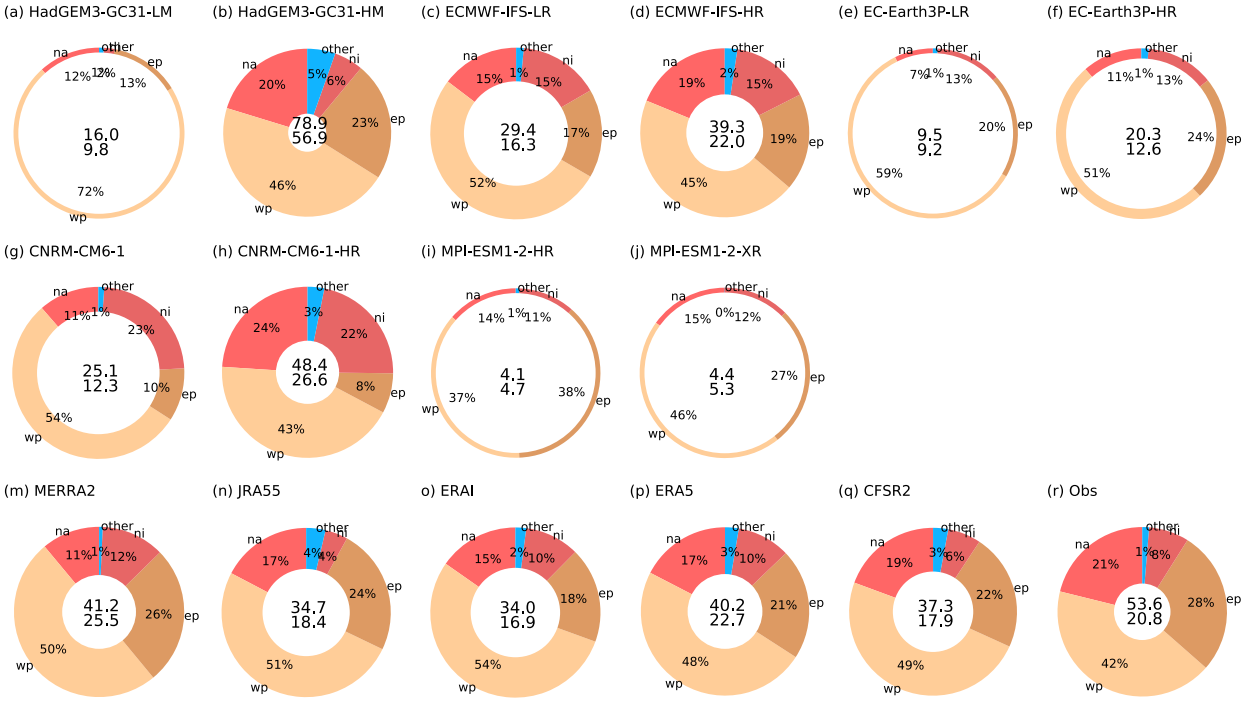

FIG. 2. As in Fig. 1, but using the TempestExtremes algorithm. Note that the required diagnostics are not available for the CMCC-CM2-(V)HR models.

- There is a common negative bias in the western Pacific, which would indicate a lack of simulated TCs making landfall in the Philippines and southern China.
- Two models—HadGEM3-GC31 and CMCC-CM2-(V)HR4, which are both gridpoint models—show a larger change with resolution, including a positive bias near the equator extending across the Pacific which is enhanced at higher resolution, and larger positive biases extending into the midlatitudes.
- The MPI-ESM1.2 model has very few TCs in any basin.

Results from TempestExtremes (not shown) have similar biases to Fig. 3, with slightly larger negative biases in the tropics and reduced positive biases in the extratropics, consistent with the lower frequencies shown in Figs. 1 and 2. The resolution differences are also similar, enhanced in HadGEM3-GC31 and CNRM-CM6.1 where the lower resolution has fewer TCs, and hence the key aspects are common to both trackers apart from the Southern Hemisphere activity.

The models tend to fall into groups of responses. The HadGEM3-GC3.1 and CMCC-CM2-(V)HR4 models show similar biases and differences with resolution, as do the EC-Earth3P and ECMWF models. The latter is probably unsurprising given the common basis of their dynamical cores, while the former are the only grid point models.

A summary of the impact of horizontal resolution on the TC spatial distribution is shown in Fig. 4, using the warm core segments of the cyclone tracks only. The multimodel ensemble mean resolution difference (Figs. 4a,b) and root-mean-square error (RMSE) difference relative to the observed track density (Figs. 4c,d) are shown for both TRACK and TempestExtremes. Both trackers have very consistent increases in track density with higher horizontal resolution, and this leads to decreases in RMSE of more than 50% in the North Atlantic and the eastern and northwestern Pacific and the southern Indian and Australian regions (blue regions in Figs. 4c and 4d).

There is a slight southward shift of activity in the eastern Pacific at higher resolution with the TRACK tracker, which causes a larger error, and the positive error toward the midlatitudes is more evident when using TRACK than TempestExtremes, consistent with the longer tracks as seen in the track densities in Fig. 3.

In summary, enhanced horizontal resolution generally reduces some typical TC biases found in CMIP-class models, and the relative improvements are consistent across two trackers. Biases remain in the southern sector of the northwestern Pacific at high resolution, which will impact TC landfall statistics there. The North Atlantic remains a challenging region to simulate (Camargo et al. 2013b), perhaps partly due to low rates of intensification (see more later in this paper; also see Manganello et al. 2012) as well as sensitivity to model physics (Bruyère et al. 2017; Chauvin et al. 2019), although the low biases are generally improved

Downloaded from http://journals.ametsoc.org/jcli/article-pdf/33/7/2557/4930746/jclid190639.pdf by guest on 08 September 2020

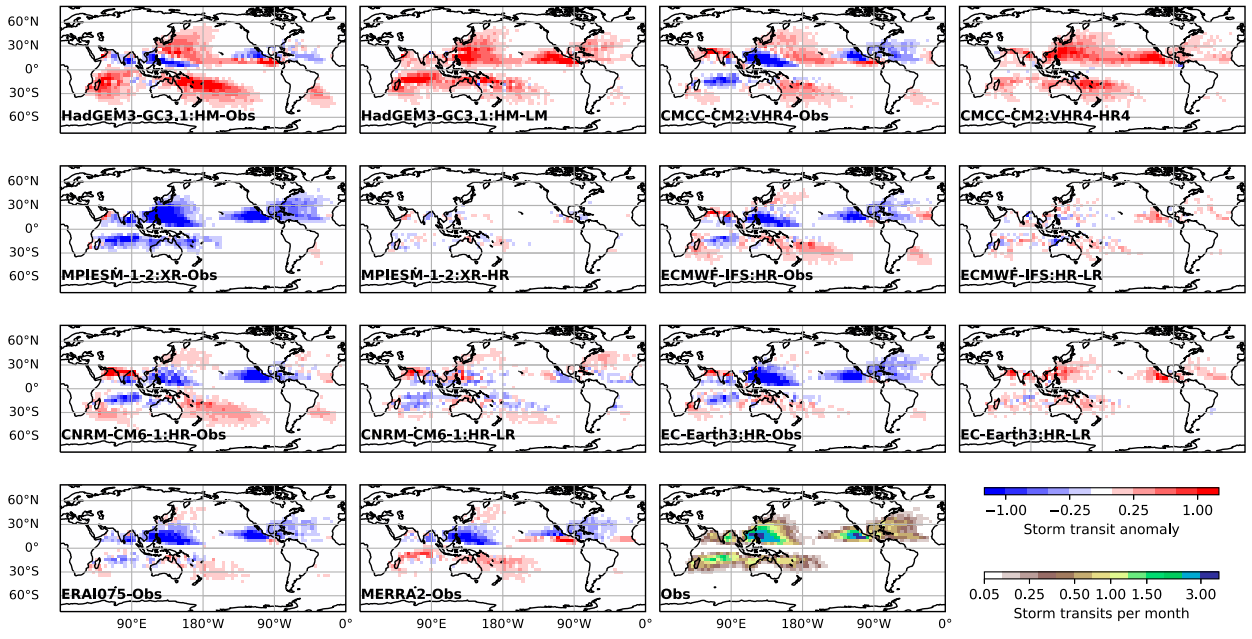

FIG. 3. Model tropical cyclone track density (storm transits per month per 4° cap): for each pair of models, the bias for the higher-resolution model and the difference between higher- and lower-resolution models are shown, respectively, in comparison with observations (last plot). The period used is 1979–2014. Note the two reanalysis products (ERA-Interim and MERRA2).

at higher resolution. Ongoing work suggests that one reason for increased TC frequency in all basins with higher horizontal resolution is a higher conversion rate of pre-TC "seeds" into TCs (Vecchi et al. 2019).

b. *Tropical cyclone intensity*

Many recent studies have indicated that although changes in aspects of future tropical cyclone climatology are uncertain, it is likely that strong storms could become stronger due to increased energy availability (in the form of increasing SSTs and column water vapor; Walsh et al. 2016). Elsner et al. (2008) suggest there is already evidence for this in the historic record, while Kossin et al. (2014) suggest an observed poleward shift to the latitude of maximum intensity, although the uniformity of the observational record is questionable

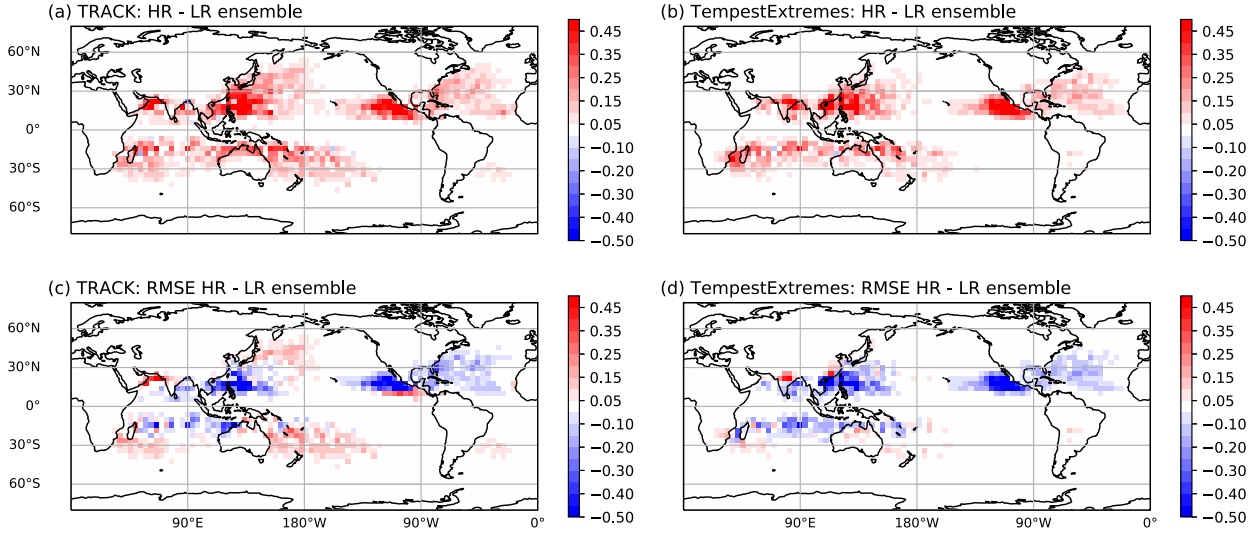

FIG. 4. Ensemble mean of the track density (a),(b) difference and (c),(d) RMSE difference between pairs of high- and low-resolution models using (left) TRACK and (right) TempestExtremes.

Downloaded from http://journals.ametsoc.org/jcli/article-pdf/33/7/2557/4930746/jclid190639.pdf by guest on 08 September 2020

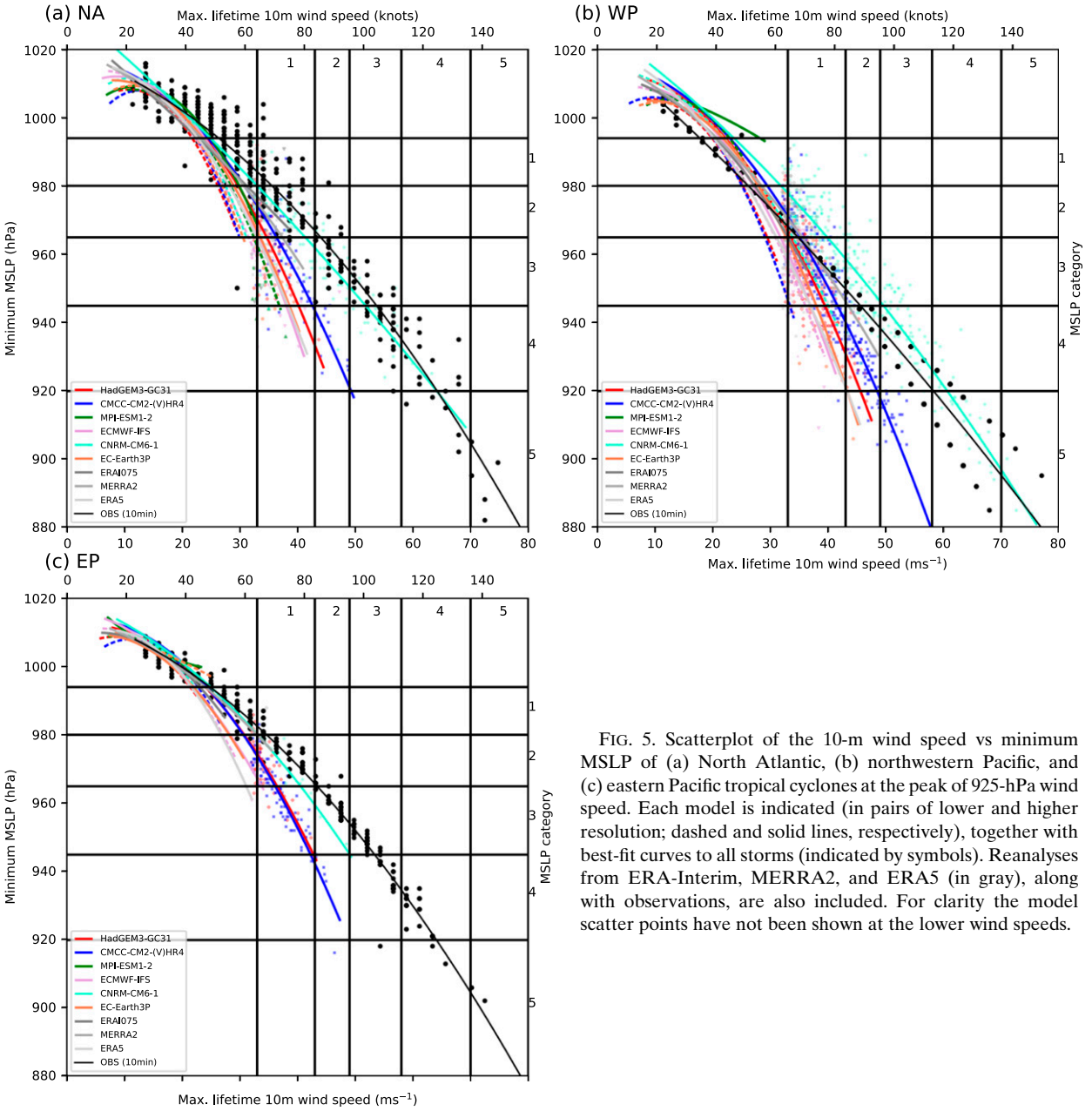

FIG. 5. Scatterplot of the 10-m wind speed vs minimum MSLP of (a) North Atlantic, (b) northwestern Pacific, and (c) eastern Pacific tropical cyclones at the peak of 925-hPa wind speed. Each model is indicated (in pairs of lower and higher resolution; dashed and solid lines, respectively), together with best-fit curves to all storms (indicated by symbols). Reanalyses from ERA-Interim, MERRA2, and ERA5 (in gray), along with observations, are also included. For clarity the model scatter points have not been shown at the lower wind speeds.

(Barcikowska et al. 2012; Ren et al. 2011). However, modeling such changes is challenging for multidecadal global climate simulations, in which the horizontal resolution is such that few models can simulate strong (category 4 or 5) hurricanes, particularly in terms of surface wind speeds (Murakami et al. 2012; Murakami et al. 2015; Wehner et al. 2014). Without this capability, drawing conclusions on changing intensities determined by wind speed is somewhat questionable, and hence here we focus on minimum surface pressure instead.

Figure 5 shows the intensity scatter and best fit [maximum 10-m wind speed vs minimum mean sea level pressure (MSLP) at peak storm intensity] for models, reanalyses, and observations, for the North Atlantic, northwestern Pacific, and eastern Pacific basins respectively. In each basin there is a systematic shift of the model intensities to higher values as resolution is increased (moving from dashed to solid lines), which is as expected; all the models struggle to achieve storm intensities much greater than category 2–3 using 10-m wind speeds apart from the CNRM-CM6.1-HR model. This model is an outlier, matching observations extremely

Downloaded from http://journals.ametsoc.org/jcli/article-pdf/33/7/2557/4930746/jcli190639.pdf by guest on 08 September 2020

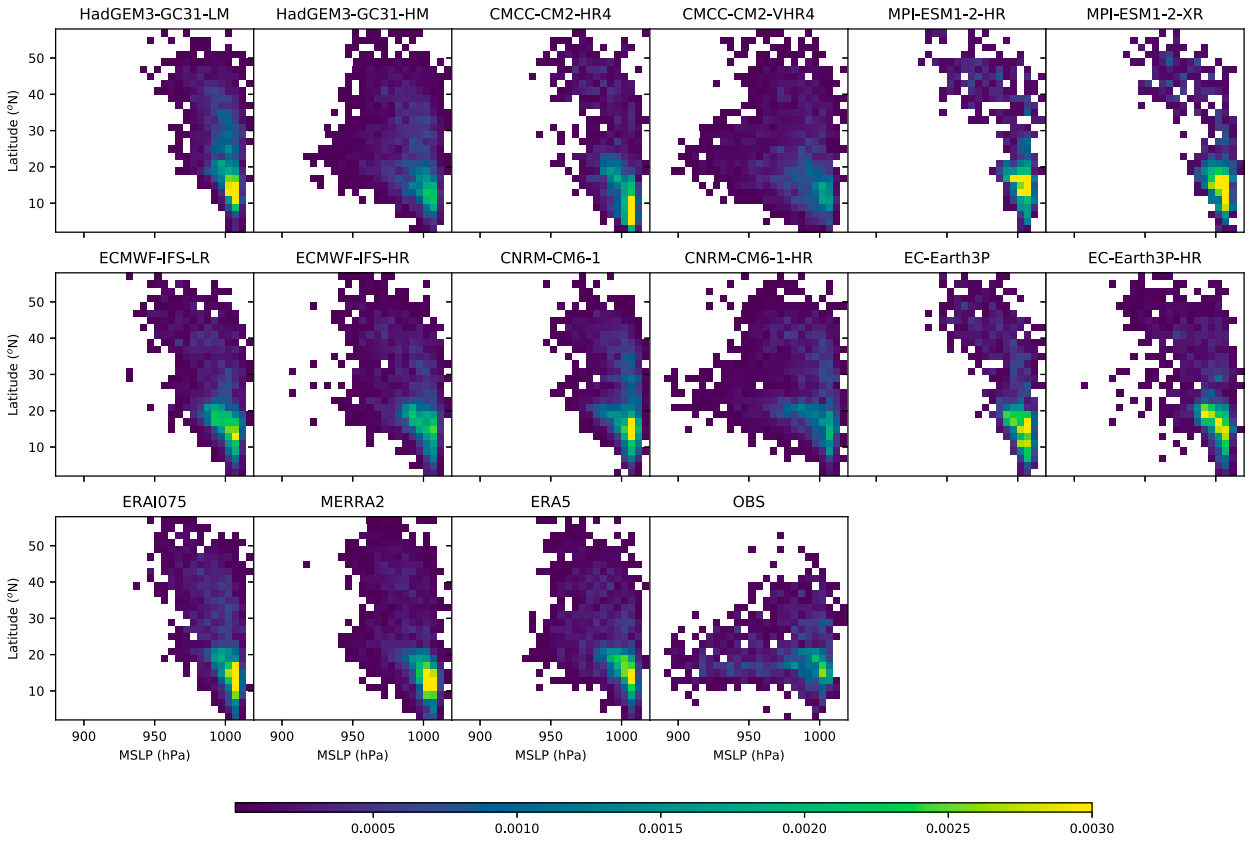

FIG. 6. Joint pdf of the normalized frequency of the MSLP and latitude at peak storm intensity from models, reanalyses, and observations for all Northern Hemisphere tropical cyclones over 1979–2014.

closely in the Atlantic and somewhat overestimating them in the northwestern Pacific.

Such strong wind speeds are beyond the expected capability of the resolved dynamics of a model at this resolution according to Davis (2018). The TC intensities in CNRM-CM6.1-HR are also very different from the previous CNRM-CM5.1 model (Voldoire et al. 2013). Understanding how this model is able to generate such strong TCs is the subject of an ongoing study (Chauvin et al. 2019; F. Chauvin et al. 2019, unpublished manuscript), but preliminary results suggest that the new Cuxart–Bougeault–Redelsperger turbulence scheme (Cuxart et al. 2000) and the coefficients therein play an important role in enhancing the TC strength via convection. This could be viewed as either a parameterization of an unresolved process, or as an outcome of parameter choices and hence perhaps as the right result for the wrong reason.

The models are able to capture the difference in storm intensities in each basin, with more frequent stronger storms in the northwestern Pacific and North Atlantic and typically weaker storms in the eastern Pacific. It is also evident here that the reanalyses also struggle to sample the more intense TC activity.

Note that TC intensity is artificially higher in these SST-forced simulations, and it has been shown that interaction with the ocean (i.e., the TC–ocean negative feedback) plays a pivotal role in reducing it (Zarzycki 2016; Scoccimarro et al. 2017c). Hence coupled model simulations are likely to produce weaker TCs.

To examine where the TCs have their peak intensity, Fig. 6 shows the joint probability density function (pdf) of the MSLP and latitude of tropical cyclones at peak intensity for all the models, reanalyses using TRACK, and observations. The observations indicate that the TCs at their peak tend to be found at latitudes between 10° and 30°N with some weaker storms found farther north. The low-resolution models cannot capture very low MSLP and hence the MSLP distribution with latitude is more uniform or even with a peak at higher latitudes. This likely reflects lower growth rates and also that at midlatitudes the model resolution becomes more suitable for the scale of the dynamics. In some of the higher-resolution models the low-latitude "bulge" is more consistent with the observations, although they still have too much activity at higher latitudes. The equivalent TempestExtremes figure (not shown) is broadly

Downloaded from http://journals.ametsoc.org/jcli/article-pdf/33/7/2557/4930746/jclid190639.pdf by guest on 08 September 2020

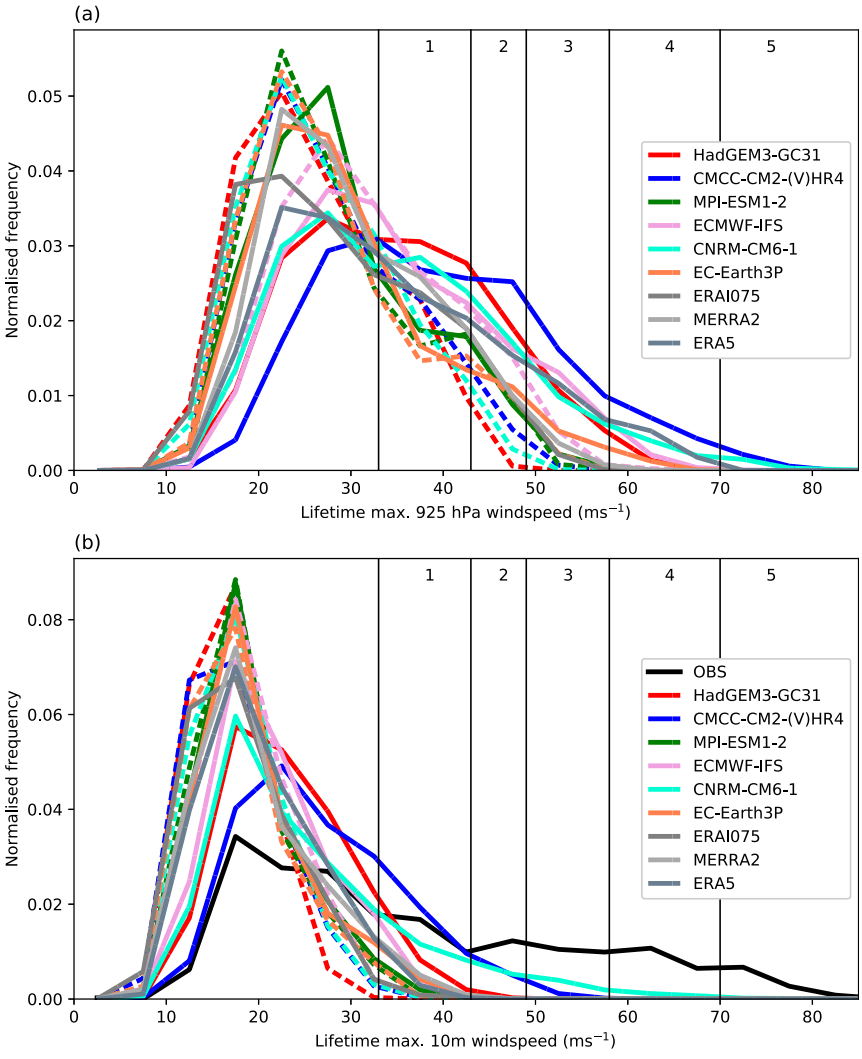

FIG. 7. Normalized pdf of wind speeds at (a) 925 hPa (vmax) and (b) 10 m, taken at the lifetime peak of the tropical cyclone intensity, for models, reanalyses, and observations for Northern Hemisphere storms. Dashed or solid lines show the low-resolution or high-resolution models, respectively.

similar, although the density of storms at higher latitudes is reduced due to the shorter tracks.

In attempting to understand the behavior of model storm intensity further, Figs. 7a and 7b show normalized pdfs of winds at both 925 hPa and 10 m from each TC at peak storm intensity for Northern Hemisphere storms. The CMCC-CM2-VHR4 and CNRM-CM6.1 HR models have maximum 925-hPa winds reaching around 80 m s^{-1} (Fig. 7a), while most of the other HR models achieve around 65 m s^{-1}. For 10-m winds, the CNRM-CM6.1 HR model has wind speeds in excess of 60 m s^{-1}, while CMCC-CM2-VHR4 reaches 55 m s^{-1} and other models more typically 40 m s^{-1}. The equivalent figure for TempestExtremes is very similar.

This would indicate that, in order for a model to attain category-4–5 10-m wind speeds, it requires both high winds at 925 hPa and for that momentum to be efficiently exchanged with the near surface via the boundary layer. More detailed process-level analysis will be required to understand whether this is a well-modeled physical process improvement (perhaps relating to boundary layer, convection, or surface drag schemes) or whether they are an indication of marginally resolving grid-scale features.

To illustrate that the storms produced in the models do indeed reflect the observed tropical cyclone structure, Fig. 8 shows composite structures of the 10-m tangential wind speeds and MSLP from the low- and

Downloaded from http://journals.ametsoc.org/jcli/article-pdf/33/7/2557/4930746/jclid190639.pdf by guest on 08 September 2020

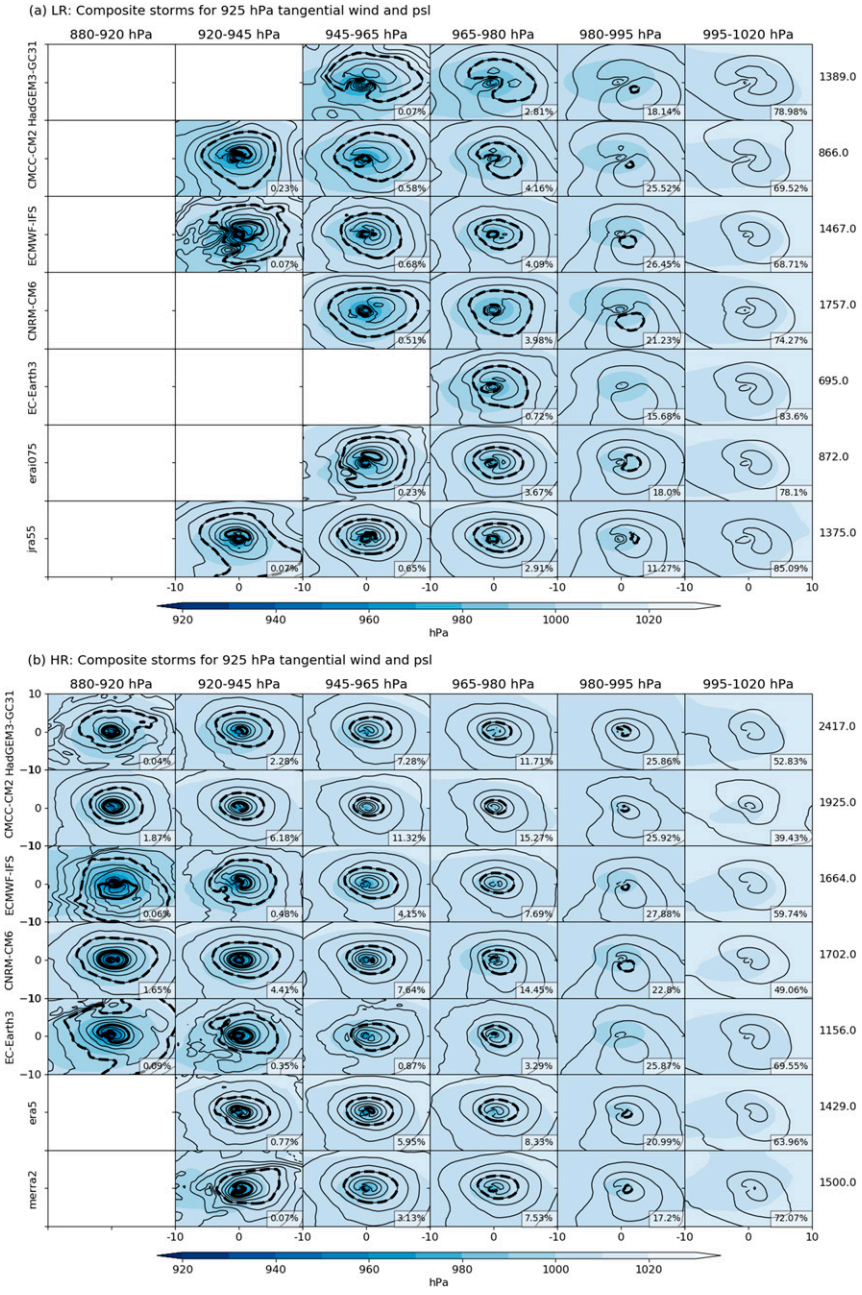

FIG. 8. Composite storm structures from (a) lower- and (b) higher-resolution models, together with ERA-Interim, JRA-55, ERA5, and MERRA2 reanalyses, stratified by minimum surface pressure at peak storm intensity. Color indicates the surface pressure, and contours show the tangential velocity at 925 hPa. The dashed contour is 20 m s^{-1}, and the solid contours are at 40 and 60 m s^{-1}. The numbers on the right are the total number of tropical cyclones over the period, of which the percentage inset indicates how many occur for each category.

high-resolution model groups and reanalyses, stratified in columns by intensity based on minimum surface pressure. The structures are broadly consistent across models, with the core becoming smaller and more intense at higher resolution as expected. The CNRM-CM6.1 HR and CMCC-CM2-VHR4 models have a larger proportion of storms contributing to the composites at the highest intensity, consistent with the results described

Downloaded from http://journals.ametsoc.org/jcli/article-pdf/33/7/2557/4930746/jcli190639.pdf by guest on 08 September 2020

above, and hence the more robust composites. Note that for some models and categories, the sample of storms can become very small.

In summary, the higher-resolution models are able to produce more intense TCs in terms of 10-m wind speed and surface pressure. Only the CNRM-CM6.1-HR model is able to simulate above category-3 10-m wind speeds, and hence these models do not have the capabilities of some other models at around 25-km resolution (Murakami et al. 2012; Murakami et al. 2015; Wehner et al. 2014).

c. North Atlantic mean frequency and seasonal cycle

The May–November mean tropical cyclone frequency in the North Atlantic from models and reanalyses using TRACK and TempestExtremes, and observations, over 1979–2014 (using the longer 1950–2014 period for the models shows only minor differences), is shown in Table 6, together with a breakdown to intensity classes (as measured by minimum SLP during storm lifetime). Common features include the following:

- The frequencies and standard deviations are mostly reduced using TempestExtremes relative to TRACK, as seen previously, and this is mainly due to a reduction in the weaker storms.
- All models (apart from HadGEM3-GC31-MM) have standard deviations that are lower than observations and reanalyses; this has implications when considering climate risks from interannual-decadal tropical cyclone variability, and it is sensitive to tracker.
- All the higher-resolution models have an increase in storms at higher intensities, with CMCC-CM2-VHR4 and CNRM-CM6.1-HR beginning to reflect similar distributions to the observations and surpassing reanalyses in this respect.
- The CNRM-CM6.1 model has a high frequency even at low resolution using TRACK with little change between resolutions, but many of these are weak storms, and with TempestExtremes the CNRM-CM6.1-LR has much lower frequency.
- Apart from MPI-ESM1.2, all of the higher-resolution models have mean TRACK TC frequency within the standard deviation of the observations (and the range as represented by the reanalysis datasets).

As seen previously, the use of TempestExtremes tends to considerably reduce the numbers of storms found, with the largest differences found in the weaker storm categories. Appendix B discusses potential reasons why the trackers may act in this way. There is some evidence that the difference between trackers reduces at higher resolution, which is an expected result given that higher resolution simulates stronger storms and tracker variability is dominated by weak, short-lived systems (Zarzycki and Ullrich 2017). The particular reasons for why some storms are detected by one tracker and not another are outside the scope of this study but remain a target for future work.

The seasonal cycle of ACE and frequency for the North Atlantic is shown in Fig. 9 for all models and reanalyses (using TRACK and ACE_{925}) and observations over 1979–2014. The peak in activity in observations is during August and September, and the ECMWF-IFS, CNRM-CM6.1, and EC-Earth3P models mirror this well. HadGEM3-GC31 and CMCC-CM2-(V)HR4 have a slightly delayed peak in September–October, and also have too much activity early in the season, which is also true of the frequency distribution. The timing of peak activity does not seem to change with model resolution for either frequency or ACE_{925}. For most models the seasonal cycle based on TempestExtremes (not shown) scales the frequency and ACE_{925} consistent with earlier results, but for HadGEM3-GC31-HM the phase error above almost disappears, which perhaps suggests that the late-season activity with TRACK is due to weaker storms.

d. Interannual variability and ensemble size

Future projections of the frequency and variability of tropical cyclones strongly depend on how the forcing environment (e.g., global and local drivers such as SST, ENSO, and humidity) will change in the future (Zhao and Held 2012; Murakami et al. 2012; Roberts et al. 2013; Sun et al. 2017). However, our confidence in model projections of future variability is increased if we can show that past performance agrees well with observations, and particularly if models have similar dependencies on both global and regional drivers as are observed. In this section we examine the importance of ensemble size and model resolution to the skill in interannual variability.

Previous studies have shown, in individual models, that higher model resolution with small ensemble sizes (Zhao et al. 2009; Roberts et al. 2015) and larger ensemble sizes at one resolution (Yoshida et al. 2017; Mei et al. 2019) are both important to capture skill in interannual variability of TCs as compared with observations. The larger ensemble sizes mean that the TC internal variability (weather noise) can be averaged out to give increasing correlation with observations (Mei et al. 2019).

In the present study the ensemble size is generally small (1–3 members) across the multimodel dataset; however, for the HadGEM3-GC31 model this has been enhanced. A total of 14 members have been produced for the period 1979–2014, at both LM and MM resolutions [see Table 1; nominally 250- and 100-km resolution, respectively, as part of the H2020 Blue-Action project

Downloaded from http://journals.ametsoc.org/jcli/article-pdf/33/7/2557/4930746/jcli190639.pdf by guest on 08 September 2020

TABLE 6. Mean tropical cyclone frequency in the North Atlantic basin during May–November 1979–2014. Mean or std indicates the mean frequency or standard deviation, respectively, of storms of all strengths; TS (tropical storm) and Cat 1P–Cat5P show the percentage of this mean value that lies within these pressure-based categories. The mean and std are shown for both TRACK and TempestExtremes (in italics and parentheses) where available.

Model	Resolution (nominal; km)	Mean, std TRACK (*Tempest*)	%TS	%Cat1P	% Cat2P	%Cat3P	%Cat4P	%Cat5P
HadGEM3-GC3.1	250	8.5; 2.7	84	12	3	0	0	0
		(1.9; 1.0)	*64*	*28*	*8*	*0*	*0*	*0*
	100	15.1; 4.6	72	21	5	2	0	0
		(9.8; 2.8)	*60*	*31*	*7*	*2*	*0*	*0*
	50	14.8; 3.3	57	24	13	6	0	0
		(16.0; 3.6)	*50*	*28*	*16*	*5*	*0*	*0*
EC-Earth	100	3.3; 2.2	84	12	3	2	0	0
		(0.7; 0.8)	*77*	*16*	*9*	*0*	*0*	*0*
	50	6.0; 3.2	81	6	6	7	0	0
		(2.3; 2.1)	*65*	*14*	*10*	*11*	*0*	*0*
CNRM-CERFACS	250	14.7; 3.5	91	7	2	0	0	0
		(2.9; 2.0)	*80*	*15*	*4*	*1*	*0*	*0*
	50	15.0; 3.1	60	16	12	9	3	0
		(12.6; 3.4)	*42*	*26*	*15*	*13*	*4*	*0*
MPI	100	2.9; 2.7	92	3	2	2	1	0
		(0.6; 0.7)	*86*	*14*	*0*	*0*	*0*	*0*
	50	2.6; 1.6	85	5	3	7	0	0
		(0.7; 1.0)	*87*	*8*	*4*	*0*	*0*	*0*
CMCC	100	3.4; 1.8	75	13	11	1	0	0
	25	9.4;3.0	49	21	12	13	5	0
ECMWF	50	7.9; 3.3	78	14	6	2	0	0
		(4.3; 2.5)	*68*	*21*	*8*	*3*	*1*	*0*
	25	10.0; 3.2	69	14	9	7	1	0
		(7.4; 3.2)	*57*	*19*	*15*	*8*	*1*	*0*
Reanalyses	ERA-Interim	8.7, 3.3	73	16	8	3	0	0
		(5.2, 3.0)	*66*	*24*	*10*	*1*	*0*	*0*
	CFSR	15.5; 4.3	85	10	4	1	0	0
		(7.2; 3.5)	*70*	*22*	*7*	*1*	*0*	*0*
	MERRA2	12.0; 4.9	69	16	13	2	0	0
		(4.7; 2.0)	*60*	*21*	*17*	*2*	*0*	*0*
	JRA-55	13.6; 4.0	76	15	8	1	0	0
		(6.0; 3.14)	*60*	*25*	*14*	*1*	*0*	*0*
	ERA5	10.9; 4.1	63	15	12	9	1	0
		(7.0; 3.5)	*46*	*24*	*17*	*11*	*1*	*0*
Obs		11.3 (4.7)	43	23	10	9	10	3

Downloaded from http://journals.ametsoc.org/jcli/article-pdf/33/7/2557/4930746/jcli190639.pdf by guest on 08 September 2020

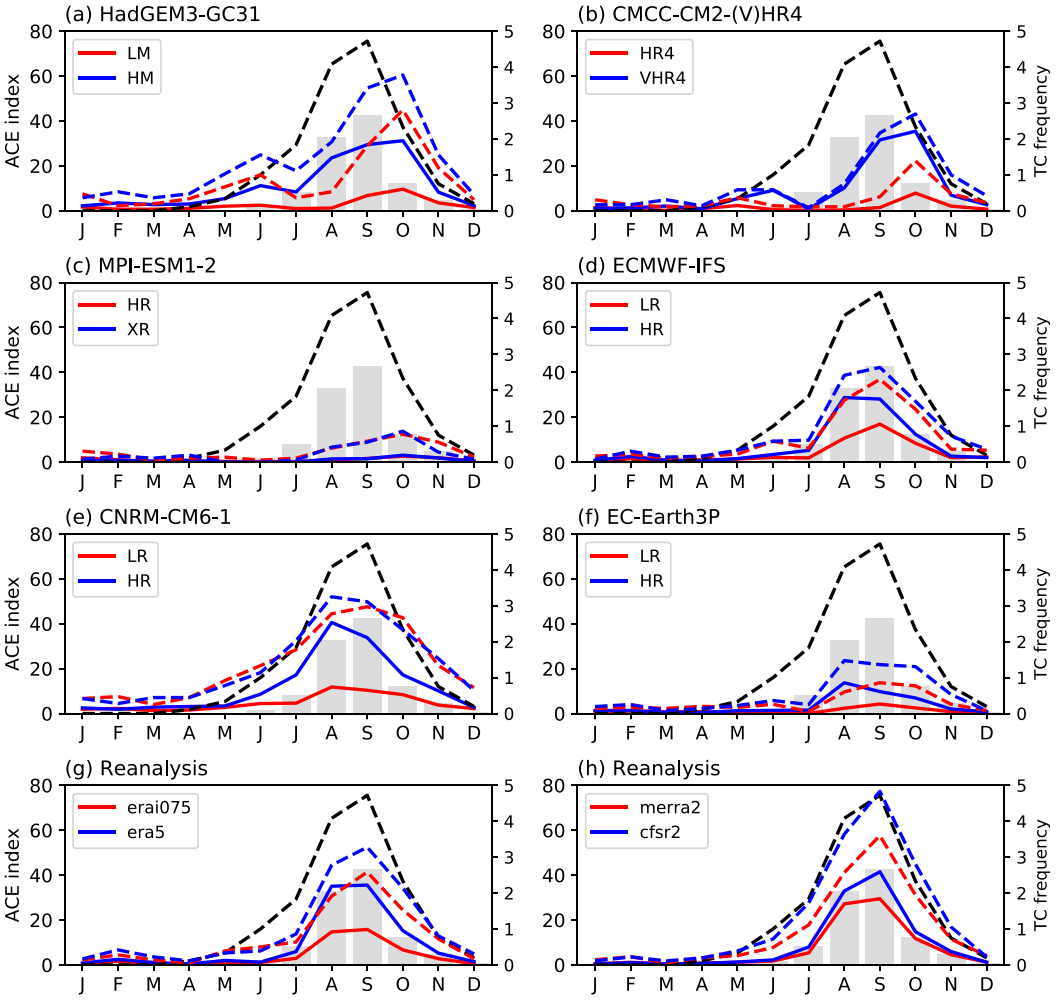

FIG. 9. Mean seasonal cycle of tropical cyclone ACE and frequency in the North Atlantic for models and reanalyses (using TRACK) and observations. In each plot, the gray bars represent the observed monthly mean ACE over the 1979–2014 period, with the solid lines representing the modeled ACE_{925}. The dashed lines show the TC frequency for observations (black) and models. The red or blue line is the lower or higher resolution, respectively, for each model or reanalysis.

(http://blueaction.eu)], together with five members at 50-km resolution. A stochastic perturbation is applied to the initial conditions to generate the ensemble. Figure 10 shows the correlation of each set of combinations of (nonindependent) n ensemble members within the whole ensemble for 1979–2014 for both frequency and ACE_{925} in the North Atlantic and the northwestern and eastern Pacific using TRACK (solid lines) and TempestExtremes (dashed lines); the box indicates the interquartile range, the whiskers show the range of the data, and the lines join the mean correlation achieved for each ensemble size. The significance levels at 95% and 99% are also indicated, based on 36 years of data.

For ACE_{925} and frequency (apart from the northwestern Pacific), the 100-km model has higher correlation than the 250-km model in all three basins using all ensemble members. It seems that at least 6–8 members selected from this ensemble size are needed for the correlations at these two resolutions to become distinct (as measured by nonoverlapping interquartile ranges). The 100-km ensemble mean correlations for frequency and ACE_{925} in the North Atlantic seem to asymptote at around 0.75 and 0.70 respectively, which for example compares to a range of correlation between 0.4 and 0.85 using particular combinations of three-member ensembles. Note that the combinations are not independent, hence the reduction in range for larger ensemble sizes. Since the 50-km model only has five ensemble members it is difficult to compare this to the lower resolutions, but there are indications that there is potentially extra ACE_{925}

Downloaded from http://journals.ametsoc.org/jcli/article-pdf/33/7/2557/4930746/jcli190639.pdf by guest on 08 September 2020

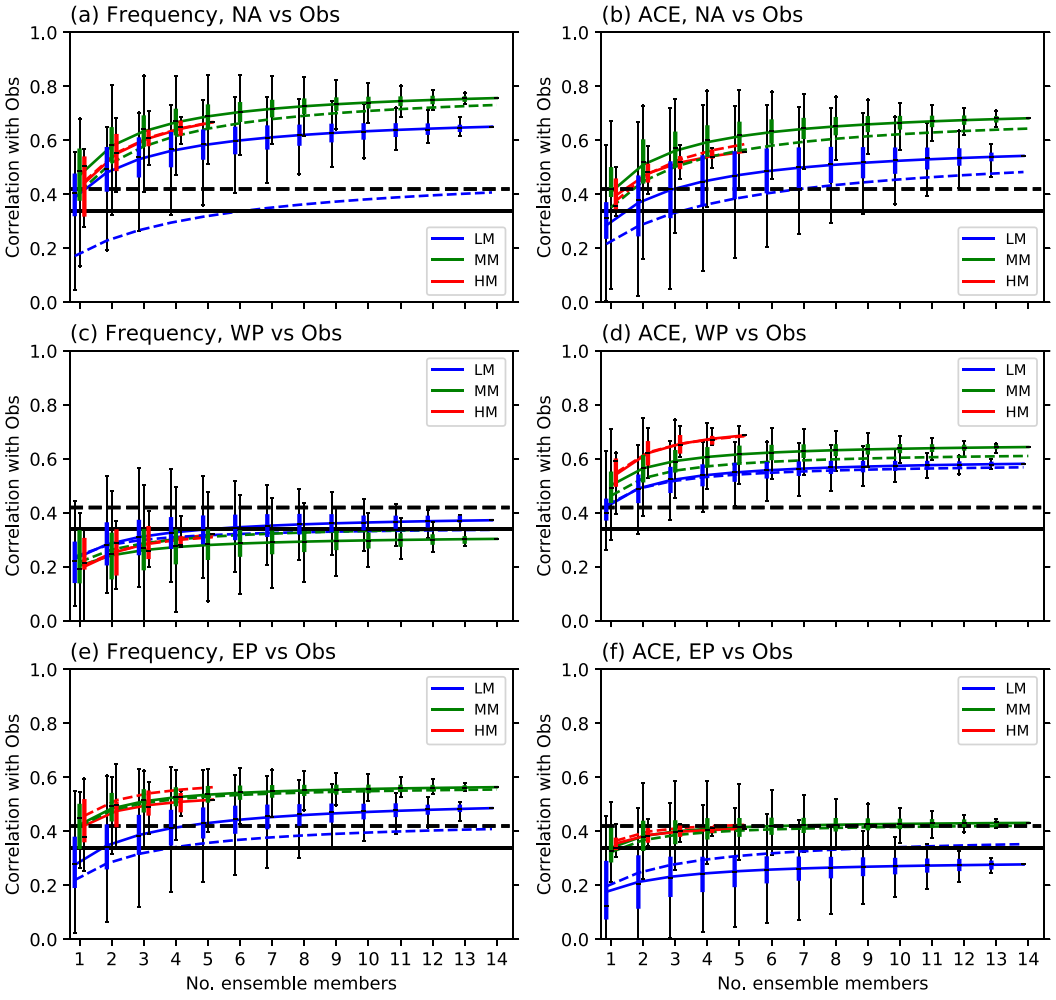

FIG. 10. Correlation of (left) model tropical cyclone frequency and (right) ACE_{925} for the (a),(b) North Atlantic (NA), (c),(d) northwestern Pacific (WP), and (e),(f) northeastern Pacific (EP) over 1979–2014 against observations for ensembles of HadGEM3-GC31 simulations [a total of 14 members at both MM (100 km) and LM (250 km) resolution, and 5 members at HM (50 km) resolution]. For each combination of n ensemble members (x axis), a box and whiskers are plotted (the box shows the lower–upper quartile range, with a line at the median, and the whiskers show the range of the data). The mean correlations for each n ensemble member correlation are joined up by the line. The solid lines are for TRACK, and the dashed lines are for TempestExtremes. The solid and dashed black lines are approximations of the 95% and 99% confidence levels, respectively (assuming that each of the 36 years is an independent sample).

skill in this model in the northwestern Pacific, in contrast to little or no improvement in hindcast skill in a coupled seasonal forecast model with similar resolutions (Scaife et al. 2019).

The correlations shown in Fig. 10 using TRACK and TempestExtremes become more similar as resolution is increased, and indeed mostly overlay each other at HM resolution. This could indicate that 1) as resolution increases, the tracker details become less important and a more common set of TCs is detected and 2) the influence of the weaker TCs on the interannual variability signal reduces as resolution increases. For the North Atlantic, Fig. 10 also shows that ACE is a more robust measure of variability (e.g., Villarini and Vecchi 2013; Scoccimarro et al. 2018), since the LM curves are closer together in Fig. 10b compared to Fig. 10a. This reflects the much smaller number of TCs detected by TempestExtremes and hence the weaker signal in terms of variability detected with that tracker using frequency alone, but the more integral ACE measure combining frequency, intensity, and lifetime is able to better sample the variability.

Mei et al. (2019) suggest that an ensemble of 20 members should be sufficient to skillfully simulate hurricane frequency in the North Atlantic (as opposed to

Downloaded from http://journals.ametsoc.org/jcli/article-pdf/33/7/2557/4930746/jclid190639.pdf by guest on 08 September 2020

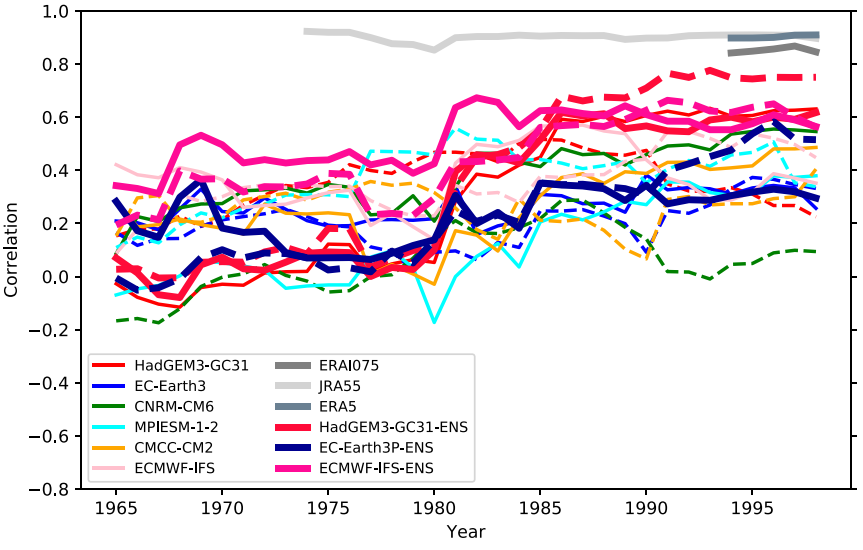

FIG. 11. Correlation of TRACK ACE_{925} from models and reanalyses for North Atlantic tropical cyclone variability against Observed ACE as a function of time, using a moving 30-yr period centered on the year shown. The dashed lines are for lower resolution, and solid lines are for higher-resolution models and reanalyses. The "-ENS" lines are for up to three member ensemble means from the available models.

tropical cyclone frequency shown here). Figure 10 suggests that more than 10 members are required to fully distinguish the skill at different model resolutions for the tropical cyclones used here, and that such an ensemble size represents most of the skill in the system (noting that some ensemble members can reach skills of over 0.8 here, perhaps indicating where the curve might asymptote to given enough members).

Since our ensemble size is much smaller in most models used here, can we say anything robust about variability and multimodel resolution? Figure 11 shows the running 30-yr correlation over the 1950–2014 period against observations for the North Atlantic, where each time series has been detrended over the whole period. There is little clear signal that the higher-resolution models obtain an improved correlation for this period using one ensemble member. It is notable that nearly all correlations improve over time, perhaps indicating that

1) the models are better in periods of increased activity and/or can detect trends in activity,
2) uncertainty exists in the SST forcing farther into the past and the methods used in HadISST.2.2.0.0 (Kennedy et al. 2017) to reconstruct the daily ¼° dataset, and
3) uncertainty exists in the tropical cyclone frequency and ACE variability before the global satellite era because of changes in observations and procedures.

The thicker lines in Fig. 11 show model ensemble means (of up to three members) where available, and these typically increase the correlation compared to using only one member. However, for two models the lower-resolution ensemble (thick dashed lines) has a greater correlation than the high-resolution ensemble (thick solid lines), suggesting either that three members is insufficient to show an improvement with resolution (consistent with Fig. 10), or else that other models could have a different resolution dependence than that shown in Fig. 10.

Table 7 shows the correlation of interannual variability with observations over the period 1979–2014 for one ensemble member for each model resolution, for both tropical cyclone frequency and ACE_{925}. For reanalyses it is clear that the ACE_{925} correlation is more robust and consistent than frequency [as shown in Villarini and Vecchi (2013) and Figs. 10a and 10b herein] and hence we focus on ACE. The models with an ensemble (of size 3 and above) have significant correlations about 0.5, whereas, of the models with only one member, only CNRM-CM6.1 at both resolutions nears 0.5.

The correlation of the TC interannual variability against selected individual drivers is shown in Table 8 for models and reanalyses. While it is difficult to assess the correlations with only one ensemble member, the models with at least three members have ensemble mean correlations that are consistent with the range seen in the reanalyses. Hence there is no reason to believe that the simulated TC variability has drivers different from the observations. The range of correlations using only one member may be simply indicative of

Downloaded from http://journals.ametsoc.org/jcli/article-pdf/33/7/2557/4930746/jcli190639.pdf by guest on 08 September 2020

TABLE 7. Correlations of Atlantic tropical cyclone interannual variability frequency and ACE_{925} from TRACK against observations, during May–November 1979–2014. Correlations (corr) shown are against all observed storms (tropical storm intensity and above) and against observed hurricanes only (≥CatP1). Correlations of ensemble means are shown where available, with the ensemble size as indicated in parentheses. Boldface type indicates significance at the 95% level.

Model	Resolution	Frequency corr (all; ≥Cat1P)	ACE corr (all; ≥Cat1P)	ACE corr (1950–2014)	ACE corr (ensemble mean)
HadGEM3-GC3.1	LM	**0.48; 0.46**	0.26; 0.26	0.23	**0.54** (14)
	MM	**0.68; 0.59**	**0.46; 0.45**	**0.35**	**0.68** (14)
	HM	0.32; **0.37**	**0.50; 0.48**	0.29	**0.56** (5)
ECMWF	LR	**0.52; 0.46**	**0.42; 0.40**	0.27	**0.52** (3)
	HR	**0.41;** 0.25	0.30; 0.26	0.34	**0.50** (3)
EC-Earth	LR	0.33; 0.13	0.27; 0.23	0.24	**0.44** (2)
	HR	**0.34**; 0.26	0.28; 0.28	0.25	0.33 (3)
CNRM-CERFACS	LR	**0.5**; **0.4**	**0.49; 0.46**	**0.45**	
	HR	0.26; 0.13	**0.48; 0.45**	0.35	
CMCC	LR	**0.54; 0.45**	0.31; 0.29	0.24	
	HR	**0.51; 0.47**	**0.37; 0.35**	0.30	
MPI-M	LR	**0.33**; 0.12	**0.34**; 0.31	0.26	
	HR	**0.52; 0.43**	**0.38; 0.37**	0.16	
Reanalyses	ERA-Interim	**0.78; 0.73**	**0.86; 0.85**		
	CFSR	0.32; **0.35**	**0.86; 0.85**		
	MERRA2	**0.78; 0.66**	**0.87; 0.85**		
	ERA5	**0.83; 0.72**	**0.91; 0.9**		
	JRA-55	**0.68; 0.70**	**0.82; 0.82**	**0.82** (1957–2014)	

internal variability, or else it may reflect that different models have TC genesis in different regions of the North Atlantic: different drivers influence particular regions, so if cyclogenesis is shifted (e.g., equatorward or westward) then these correlations will differ from the observed.

e. Impact of mean state in the Atlantic

Simple relationships between simulated mean state, model bias, and TC climatology are generally difficult to establish (e.g., Camargo et al. 2013b; Murakami et al. 2014; Tang and Camargo 2014; Kim et al. 2018) and are often model dependent. Here we briefly examine whether the models show any gross biases in key parameters known to be important for TC performance.

The mean 850–250-hPa wind shear over the June–October period for 1979–2014 is shown in Fig. 12 for models and reanalyses. Each model tends to have its own pattern of shear, and there seems little systematic change with resolution. The CNRM-CM6.1 model has the weakest shear across the North Atlantic, which is consistent with their large number of TCs produced at both resolutions using TRACK. The HadGEM3-GC31 model has its minimum shear farther south than observed, and this may be linked with the low latitude of the African easterly jet (AEJ) in that model (Fig. 13). The MPI-ESM1.2 and ECMWF-IFS models have slightly higher shear (in the eastern Atlantic) at higher resolution. The shear over West Africa and the eastern Atlantic is too high in CMCC-CM2-(V)HR4.

In general the latitudes of the AEJ (Fig. 13a) are consistent with the shear, with several models (e.g., MPI-ESM1.2) having the mean jet somewhat farther north than indicated by the reanalyses, while HadGEM3-GC31-LM is too far to the south. Some previous work (Patricola et al. 2018) has suggested that African easterly waves (AEWs) play little role in setting North Atlantic tropical cyclone numbers, while Thorncroft and Hodges (2001) and Roberts et al. (2015) showed some relationship with TC variability at higher resolutions for storms with genesis in the eastern Atlantic. The mean number of AEWs is shown in Fig. 13b, and the maximum vorticity of these waves in Fig. 13c, calculated following the Bain et al. (2014) simple Hovmöller algorithm calculated on a common grid. There is little evident resolution sensitivity in mean AEW number, and no obvious relation with each model having its own character. All the models are within the range of the reanalyses. There is a more systematic increase in the vorticity of the AEWs with model resolution and perhaps this helps to improve the storm distribution in the eastern Atlantic (Fig. 3) by enabling earlier genesis.

4. Conclusions

The CMIP6 HighResMIP experimental design enables a more systematic assessment of the role of horizontal resolution in the simulation of global tropical cyclones over the period 1950–2014 across multiple models. The results from six modeling groups within the European PRIMAVERA project have been analyzed in this work, with resolutions

Downloaded from http://journals.ametsoc.org/jcli/article-pdf/33/7/2557/4930746/jcli190639.pdf by guest on 08 September 2020

TABLE 8. Correlations of the Atlantic tropical cyclone interannual ACE_{925} variability from TRACK for the North Atlantic (May–November 1979–2014) with some potential drivers of that variability [Niño-3.4 index, Atlantic multidecadal oscillation (AMO), and Atlantic meridional mode (AMM)] for each model resolution. The ensemble mean correlations (where available) are shown in parentheses; ensemble size is as in Table 7. Boldface type indicates significance at the 95% level.

Model	Niño-3.4 ACE member 1 (ensemble mean)	AMO member 1 (ensemble mean)	AMM member 1 (ensemble mean)
HadGEM3-GC3.1			
LM	−0.3 (**−0.55**)	0.28 (0.37)	**0.4** (**0.56**)
MM	**−0.45** (**−0.55**)	0.29 (**0.53**)	**0.38** (**0.70**)
HM	−0.25 (**−0.41**)	**0.41** (**0.41**)	**0.58** (**0.62**)
ECMWF			
LR	−0.26 (**−0.46**)	0.23 (0.34)	**0.43** (**0.56**)
HR	**−0.51** (−0.40)	0.22 (0.37)	0.27 (**0.48**)
EC-Earth			
LR	−0.18 (−0.28)	0.19 (0.32)	0.23 (**0.43**)
HR	−0.03 (−0.19)	0.35 (0.28)	0.35 (0.34)
CNRM			
LR	−0.22	0.27	0.31
HR	−0.27	0.15	0.34
CMCC			
LR	−0.15	0.10	0.26
HR	**−0.41**	**0.41**	**0.42**
MPI			
LR	**−0.40**	0.10	0.25
HR	−0.10	**0.40**	**0.40**
ERA-Interim	**−0.42**	**0.56**	**0.64**
MERRA2	**−0.41**	**0.63**	**0.74**
CFSR	**−0.49**	**0.45**	**0.58**
JRA-55	**−0.44**	0.39	**0.55**
ERA5	**−0.42**	**0.56**	**0.65**

spanning from around 200 to 25 km. There are several seemingly consistent changes when resolution is increased:

- increased tropical cyclone frequency and seasonal ACE index in the North Atlantic,
- improved capability to represent the spectrum of tropical cyclone intensities, and
- improved distribution of tropical cyclone tracks (and genesis regions).

These conclusions seem to be robust to (at least two) different trackers used in this study, TRACK and TempestExtremes. These improvements are consistent with previous studies using multidecadal simulations of individual climate models at similar 25-km resolutions (e.g., Zhao et al. 2009; Caron et al. 2011; Murakami et al. 2012; Wehner et al. 2014; Murakami et al. 2015; Roberts et al. 2015).

Correlations of interannual ACE variability with observations seem to be more robust than using simple storm frequency, but there is no obvious relationship between increased resolution and improved correlation using only one ensemble member.

Using the HadGEM3-GC3.1 model and several resolutions with an ensemble of 14 members does indicate that increasing resolution from 200 to 100 km improves model skill for North Atlantic interannual variability. In this case, at 100-km resolution the ensemble mean correlation tends toward ~0.75/0.7 (frequency/ACE), with a subsample of ensemble size of 6–8 suggestive of being sufficient to be a robust measure. Hence for this simulation protocol and model, we can explain ~50% of the variance in observed tropical cyclone interannual ACE variability. In the northwestern Pacific, there is evidence that 50-km resolution offers a further increase in skill.

Future work is needed to discover what factors are missing that could allow more of the variance to be explained. This may lie within the HighResMIP protocol itself (which, e.g, excludes interannual variations in natural aerosol and uses one specific set of SST–sea ice forcing datasets) or could lie with the models themselves (via model bias, lack of key processes, requirement for even higher resolution, or limitations in physics such as convection schemes).

Further investigation of the CNRM-CM6.1 model is required to understand how it is able to achieve such outstanding surface wind speeds compared to all other models, which allows this model to represent the full tropical cyclone intensity spectrum. The other models in this study are not able to simulate above category-3 intensities as measured by 10-m wind speeds. Davis (2018) suggest that somewhat higher intensities should be possible in theory at 25-km resolution, and indeed other models have shown such capability (e.g., Wehner et al. 2014; Murakami et al. 2015).

Use of the CMIP6 HighResMIP coupled model simulations can be used to further assess drivers of variability and intensity when the atmosphere and ocean are able to fully interchange fluxes. This configuration may also be useful to understand likely future changes in tropical cyclone characteristics, and is addressed by M. Roberts et al. (2019, unpublished manuscript).

Additional assessment of different tracking trackers is needed to better understand their strengths and weaknesses and sources of difference but this needs to be done fairly with some well-constrained criteria for evaluation. Using multiple trackers is also likely to be important when assessing future climate simulations, which also form a part of the HighResMIP experimental design.

Acknowledgments. Authors MR, JS, PLV, KH, BV, RH, AB, ES, LPC, LT, CR, RS, and DP acknowledge funding from the PRIMAVERA project, funded by the

Downloaded from http://journals.ametsoc.org/jcli/article-pdf/33/7/2557/4930746/jcli190639.pdf by guest on 08 September 2020

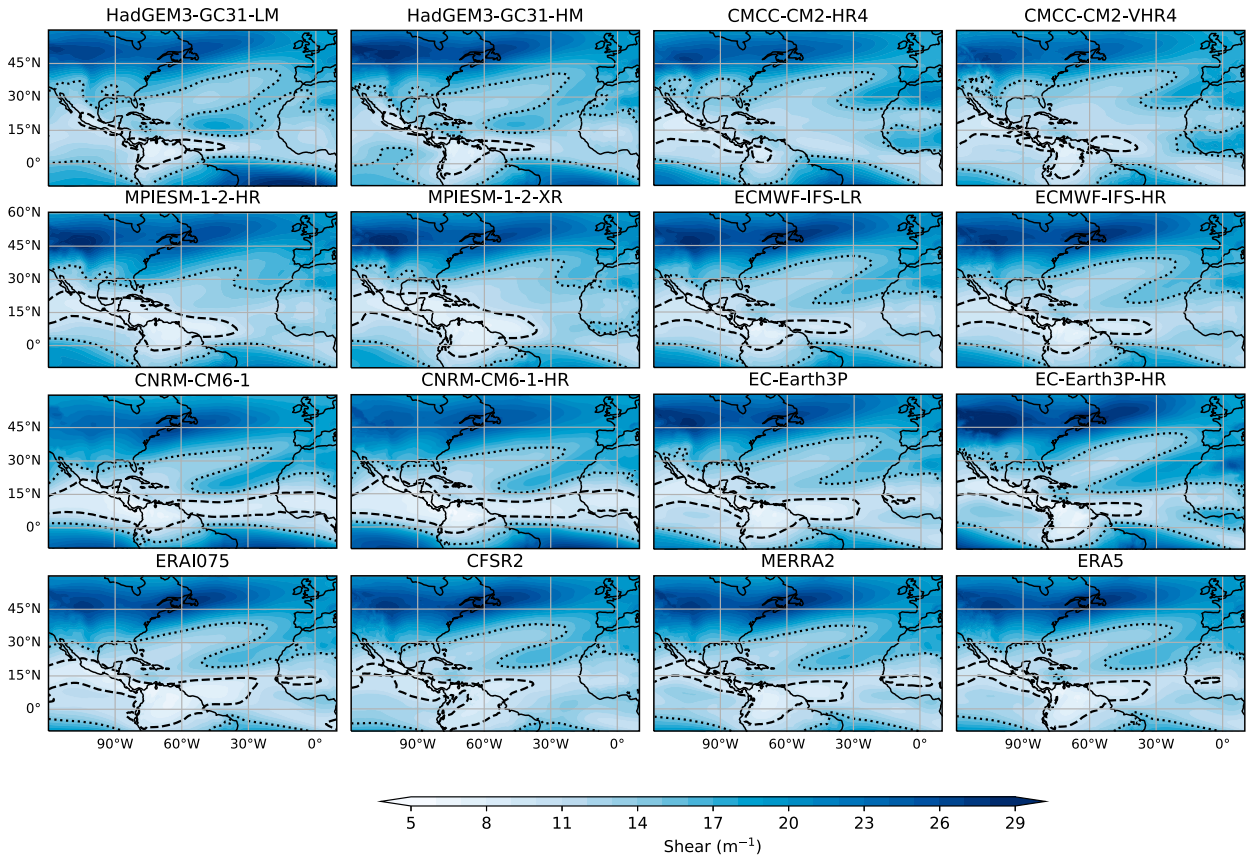

FIG. 12. Wind shear between 850 and 250 hPa for models and reanalyses for the mean over July–October 1980–2013. The dashed line shows 10 m s^{-1}, and the dotted line shows 20 m s^{-1}.

European Union's Horizon 2020 programme under Grant Agreement 641727. Author JM acknowledges funding from the Blue-Action project, funded by the European Union's Horizon 2020 programme under Grant Agreement 727852. Authors MR and JC acknowledge support from the U.K.–China Research and Innovation Partnership Fund through the Met Office Climate Science for Service Partnership (CSSP) China as part of the Newton Fund. Funding for authors PU and CZ to support use of the TempestExtremes suite was provided under NASA award NNX16AG62G and the U.S. Department of Energy Office of Science award DE-SC0016605. Many thanks are given to the editor and three anonymous reviewers for their comments, which have greatly strengthened this paper.

APPENDIX A

Brief Model Descriptions

Brief descriptions of the different models used in this study are included here, in particular aspects that are relevant to tropical cyclones. A summary of the model components is shown in Table 1, and all the parameter changes between model resolutions are shown in Table 3.

The standard HadGEM3-GC31 model configuration is described in Williams et al. (2017), with the atmosphere configuration (GA7.1) further described by Walters et al. (2019) and the HighResMIP configuration in P. Vidale et al. (2019, unpublished manuscript) and Roberts et al. (2019). The dynamical core uses a semi-implicit semi-Lagrangian formulation to solve the nonhydrostatic, fully compressible deep-atmosphere equations of motion (Wood et al. 2014) on a regular latitude–longitude grid, with 85 levels with a top at 85 km. This model has been used to generate a larger ensemble size (of up to 14 members) to examine the robustness of some results. Each resolution has at least three ensemble members over 1950–2014. In addition, over the 1979–2014 period, stochastic perturbation of the initial conditions is used and 10 additional members are produced for LM and MM models, and two more members for HM.

The ECMWF-IFS model used for HighResMIP is documented in Roberts et al. (2018) and references therein. The atmospheric component of the Integrated

Downloaded from http://journals.ametsoc.org/jcli/article-pdf/33/7/2557/4930746/jcli190639.pdf by guest on 08 September 2020

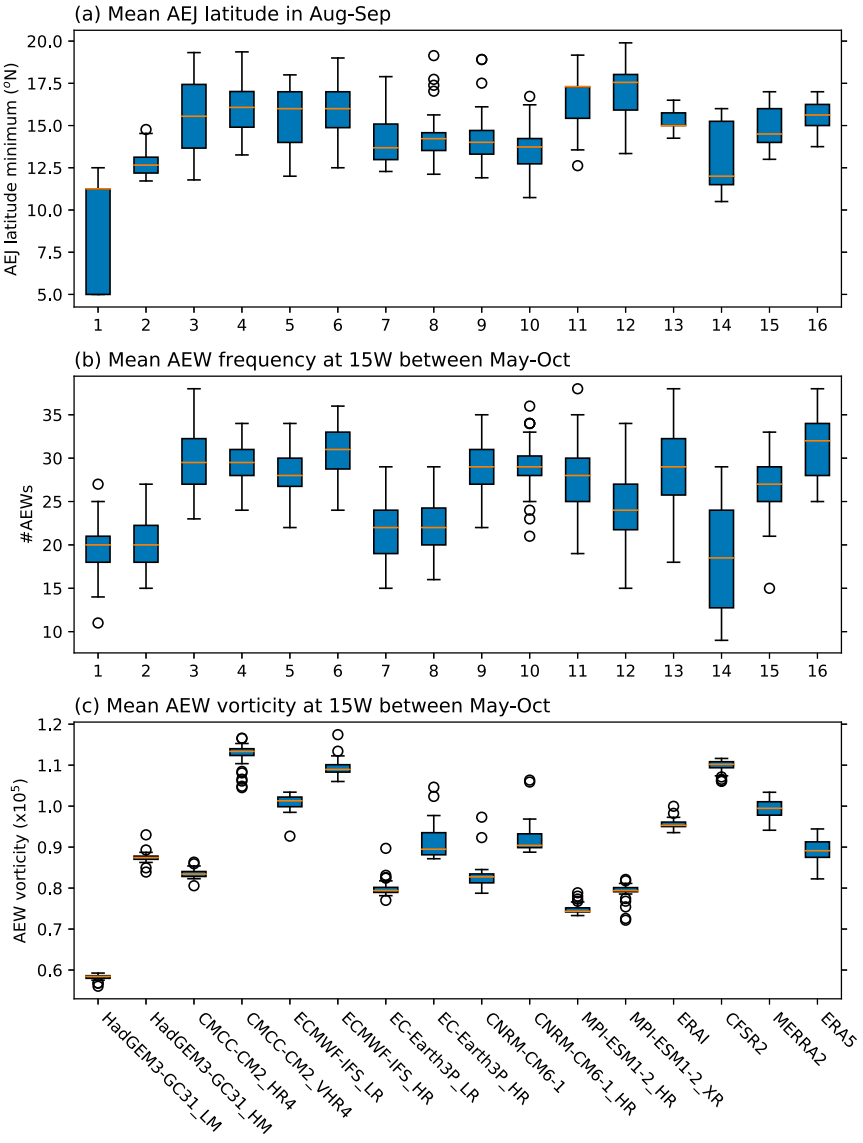

FIG. 13. (a) African easterly jet mean latitude in August–September for each model and reanalysis over 1980–2014. (b) Mean number of African easterly waves over May–October for each model, counted at 15°W using the algorithm described in Bain et al. (2014). (c) AEW vorticity at 15°W using the algorithm described in Bain et al. (2014).

Forecasting System (IFS cyc43r1) model is based on a hydrostatic, semi-Lagrangian, semi-implicit dynamical core with computations alternated between spectral and reduced Gaussian grid point representations each time step. The vertical discretization is based on a hybrid sigma-pressure coordinate, with 91 levels in the vertical, with a top at 0.01 hPa. Additional ensemble members have been generated by random perturbations to the initial stochastic perturbed parameterized tendencies (SPPT) scheme.

The EC-Earth3P model is documented in Haarsma et al. (2019, manuscript submitted to *Geosci. Model Dev.*). The atmospheric component of the Integrated Forecasting System (IFS cyc36r4) model is based on a hydrostatic, semi-Lagrangian, semi-implicit dynamical core. The vertical discretization is based on a hybrid sigma-pressure coordinate, with 91 levels in the vertical direction, with top at 0.01 hPa.

The MPI-ESM1.2 model is documented in Gutjahr et al. (2019) and references therein. The atmospheric submodel of MPI-ESM1.2 is ECHAM6.3, with a dynamical core based on a vorticity and divergence form of the primitive equations, solved using a spectral-transform method. The vertical discretization uses a hybrid

Downloaded from http://journals.ametsoc.org/jcli/article-pdf/33/7/2557/4930746/jcli190639.pdf by guest on 08 September 2020

sigma-pressure coordinate system with 95 vertical levels with a top at 0.01 hPa.

The CNRM-CM6.1 model is documented in Voldoire et al. (2019) for CMIP6 DECK experiments. It is based on four main components for atmosphere, surface, and ocean, and sea ice. The atmospheric component is based on the spectral atmospheric model ARPEGE-Climat, version 6.3. There are 91 vertical levels following a hybrid σ pressure discretization with 15 levels in the boundary layer. Since the previous version of the model, changes have been introduced in the parameterizations and mainly concern the convection (Piriou et al. 2007; Guérémy 2011), microphysics (Lopez 2002), and turbulence (Cuxart et al. 2000). The surface component SURFEX (Masson et al. 2013) includes three surface types: ocean, land, and lakes.

A general description of CMCC-CM2 models family used in CMIP6 can be found in Cherchi et al. (2019). In the present study, the CMCC-CM2-(V)HR4 configuration is used, specifically developed for HighResMIP. This model differs from the standard resolution CMCC-CM2 configuration (CMCC-CM2-SR5; Cherchi et al. 2019) in that it makes use of the Community Atmosphere Model vn4 (CAM4; Neale et al. 2010) rather than CAM5. This choice allowed a substantial reduction of computational costs, especially beneficial for the high-resolution (CMCC-CM2-VHR4) experiments, and it made possible the implementation of the MACv2-SP "simple plume" scheme for the anthropogenic aerosols (Stevens et al. 2017), following the HighResMIP protocol. Specific aspects concerning the CMCC-CM2-(V)HR4 ability in reproducing the characteristics of TCs in the western North Pacific are documented by Scoccimarro et al. (2020).

APPENDIX B

Brief Tracking Algorithm (Tracker) Descriptions

Brief descriptions of the two trackers used to find tropical cyclones within the model simulations are included here, for TRACK (Hodges et al. 2017) and TempestExtremes (Ullrich and Zarzycki 2017; Zarzycki and Ullrich 2017). There are no changes in the trackers used between models and resolutions. Note that the variables used are on the analysis grid (Table 2) for each model.

TRACK uses relative vorticity as the feature-tracking variable. The vorticity over 850, 700, and 600 hPa is averaged on the analysis grid, and then spectrally filtered to a common T63 grid using triangular truncation to retain wavenumbers 6–63. The tracking proceeds by identifying the off-grid vorticity maxima, by applying a maximization scheme (Hodges 1995), if they exceed a value of $5 \times 10^{-6}\,s^{-1}$ in each time frame (SH scaled by -1). These are initially linked together using a nearest-neighbor approach and then refined by minimizing a cost function for track smoothness, subject to adaptive constraints on displacement distance and track smoothness (Hodges 1999). Only tracks that last at least 2 days (eight time steps) are retained for further analysis. Identification criteria post tracking are used to isolate warm-core tropical cyclones: 1) T63 relative vorticity at 850 hPa must attain a threshold of $6 \times 10^{-5}\,s^{-1}$; 2) the difference in vorticity between 850 and 250 hPa (at T63 resolution) must be greater than $6 \times 10^{-5}\,s^{-1}$ to provide evidence of a warm core; 3) the T63 vorticity center must exist at each level (850, 700, 600, 500, and 250 hPa) for a coherent vertical structure; 4) criteria 1–3 must be jointly attained for at least four consecutive time steps (one day) and only apply over the oceans; and 5) tracks must start between 30°S and 30°N.

TempestExtremes uses sea level pressure (SLP) as its feature-tracking variable on the native analysis grid. Candidates are initially identified by minima in SLP, and a closed contour criterion is applied, requiring an increase in SLP of at least 2 hPa within 5.5° of the candidate node. A decrease in geopotential height difference (250–500 hPa) of 6 m within 6.5° of the candidate within 1° of the candidate with maximum geopotential height. Candidates are then stitched in time to form paths, with a maximum distance between candidates of 8°, consisting of at least 10 candidates per path and with a maximum gap size of three (number of time steps where no identification occurred). For at least 10 time steps the underlying topographic height must be at most 1500 m, and for at least four time steps it must be at most 10 m, and the storm must form between 10° and 40°. The storm must also travel at least 8°.

The TRACK configuration is tuned to capture roughly the number of tropical storms including possibly tropical depressions and subtropical storms found in observations, primarily using the ECMWF operational analyses (Bengtsson et al. 2007). The TempestExtremes configuration was developed by performing a sensitivity analysis and optimizing against high-resolution reanalysis products as described in Zarzycki and Ullrich (2017). It has attempted to keep the false-alarm rate to acceptable levels, which may have the effect of reducing the detection of weaker storms.

REFERENCES

Aon Benfield, 2018: Global economic losses. Weather, climate & catastrophe insight—2017 annual report. Aon Benfield UCL Hazard Research Centre Rep., 2–5, http://thoughtleadership.aonbenfield.com/Documents/20180124-ab-if-annual-report-weather-climate-2017.pdf.

Bain, C. L., K. D. Williams, S. F. Milton, and J. T. Heming, 2014: Objective tracking of African easterly waves in Met Office

Downloaded from http://journals.ametsoc.org/jcli/article-pdf/33/7/2557/4930746/jcli190639.pdf by guest on 08 September 2020

models. *Quart. J. Roy. Meteor. Soc.*, **140**, 47–57, https://doi.org/10.1002/qj.2110.

Barcikowska, M., F. Feser, and H. von Storch, 2012: Usability of best track data in climate statistics in the western North Pacific. *Mon. Wea. Rev.*, **140**, 2818–2830, https://doi.org/10.1175/MWR-D-11-00175.1.

Batté, L., and F. J. Doblas-Reyes, 2015: Stochastic atmospheric perturbations in the EC-Earth3 global coupled model: Impact of SPPT on seasonal forecast quality. *Climate Dyn.*, **45**, 3419–3439, https://doi.org/10.1007/s00382-015-2548-7.

Bell, G. D., and Coauthors, 2000: Climate assessment for 1999. *Bull. Amer. Meteor. Soc.*, **81** (6), S1–S50, https://doi.org/10.1175/1520-0477(2000)81[s1:CAF]2.0.CO;2.

Bengtsson, L., K. I. Hodges, and M. Esch, 2007: Tropical cyclones in a T159 resolution global climate model: Comparison with observations and re-analyses. *Tellus*, **59A**, 396–416, https://doi.org/10.1111/j.1600-0870.2007.00236.x.

Bruyère, C. L., and Coauthors, 2017: Impact of climate change on Gulf of Mexico hurricanes. NCAR Tech. Note NCAR/TN-535+STR, 165 pp., https://doi.org/10.5065/D6RN36J3.

Camargo, S. J., 2013a: Tropical cyclones in high-resolution climate models. *U.S. CLIVAR Variations*, Vol. 11, No. 3, U.S. CLIVAR Project Office, Washington, DC, 4–11, https://usclivar.org/sites/default/files/USCLIVAR_VARIATIONS_11_3_Fall2013.pdf.

——, 2013b: Global and regional aspects of tropical cyclone activity in the CMIP5 models. *J. Climate*, **26**, 9880–9902, https://doi.org/10.1175/JCLI-D-12-00549.1.

——, and A. A. Wing, 2016: Tropical cyclones in climate models. *Wiley Interdiscip. Rev.: Climate Change*, **7**, 211–237, https://doi.org/10.1002/wcc.373.

Camp, J., M. Roberts, C. MacLachlan, E. Wallace, L. Hermanson, A. Brookshaw, A. Arribas, and A. A. Scaife, 2015: Seasonal forecasting of tropical storms using the Met Office GloSea5 seasonal forecast system. *Quart. J. Roy. Meteor. Soc.*, **141**, 2206–2219, https://doi.org/10.1002/qj.2516.

Caron, L.-P., and C. G. Jones, 2012: Understanding and simulating the link between African easterly waves and Atlantic tropical cyclones using a regional climate model: The role of domain size and lateral boundary conditions. *Climate Dyn.*, **39**, 113–135, https://doi.org/10.1007/s00382-011-1160-8.

——, ——, and K. Winger, 2011: Impact of resolution and downscaling technique in simulating recent Atlantic tropical cyclone activity. *Climate Dyn.*, **37**, 869–892, https://doi.org/10.1007/s00382-010-0846-7.

Chauvin, F., R. Pilon, P. Palany, and A. Belmadani, 2019: Future changes in Atlantic hurricanes with the rotated-stretched ARPEGE-Climat at very high resolution. *Climate Dyn.*, **54**, 947–972, https://doi.org/10.1007/s00382-019-05040-4.

Cherchi, A., and Coauthors, 2019: Global mean climate and main patterns of variability in the CMCC-CM2 coupled model. *J. Adv. Model. Earth Syst.*, **11**, 185–209, https://doi.org/10.1029/2018MS001369.

Chu, J. H., C. R. Sampson, A. S. Levine, and E. Fukada, 2002: The Joint Typhoon Warning Center tropical cyclone best-tracks, 1945–2000. Naval Research Laboratory Tech. Rep. NRL/MR/7540-02-16, https://www.metoc.navy.mil/jtwc/products/best-tracks/tc-bt-report.html.

Copernicus Climate Change Service, 2017: ERA5: Fifth generation of ECMWF atmospheric reanalyses of the global climate. Copernicus Climate Change Service Climate Data Store (CDS), accessed 15 March 2019, https://doi.org/10.24381/cds.bd0915c6.

Cuxart, J., P. Bougeault, and J. L. Redelsperger, 2000: A turbulence scheme allowing for mesoscale and large-eddy simulations. *Quart. J. Roy. Meteor. Soc.*, **126**, 1–30, https://doi.org/10.1002/qj.49712656202.

Davis, C. A., 2018: Resolving tropical cyclone intensity in models. *Geophys. Res. Lett.*, **45**, 2082–2087, https://doi.org/10.1002/2017GL076966.

Dee, D. P., and Coauthors, 2011: The ERA-Interim reanalysis: Configuration and performance of the data assimilation system. *Quart. J. Roy. Meteor. Soc.*, **137**, 553–597, https://doi.org/10.1002/qj.828.

EC-Earth, 2018a: EC-Earth-Consortium EC-Earth3P model output prepared for CMIP6 HighResMIP. Earth System Grid Federation. Earth System Grid Federation, accessed August 2019, https://doi.org/10.22033/ESGF/CMIP6.2322.

——, 2018b: EC-Earth-Consortium EC-Earth3P-HR model output prepared for CMIP6 HighResMIP. Earth System Grid Federation. Earth System Grid Federation, accessed August 2019, https://doi.org/10.22033/ESGF/CMIP6.2323.

Elsner, J. B., J. P. Kossin, and T. H. Jagger, 2008: The increasing intensity of the strongest tropical cyclones. *Nature*, **455**, 92–95, https://doi.org/10.1038/nature07234.

Eyring, V., S. Bony, G. A. Meehl, C. Senior, B. Stevens, R. J. Stouffer, and K. E. Taylor, 2016: Overview of the Coupled Model Intercomparison Project Phase 6 (CMIP6) experimental design and organisation. *Geosci. Model Dev.*, **9**, 1937–1958, https://doi.org/10.5194/gmd-9-1937-2016.

Franco-Díaz, A., N. P. Klingaman, P. L. Vidale, L. Guo, and M.-E. Demory, 2019: The contribution of tropical cyclones to the atmospheric branch of Middle America's hydrological cycle using observed and reanalysis tracks. *Climate Dyn.*, **53**, 6145–6158, https://doi.org/10.1007/s00382-019-04920-z.

Gelaro, R., and Coauthors, 2017: The Modern-Era Retrospective Analysis for Research and Applications, version 2 (MERRA-2). *J. Climate*, **30**, 5419–5454, https://doi.org/10.1175/JCLI-D-16-0758.1.

Guérémy, J. F., 2011: A continuous buoyancy based convection scheme: One- and three-dimensional validation. *Tellus*, **63A**, 687–706, https://doi.org/10.1111/j.1600-0870.2011.00521.x.

Guo, L., N. P. Klingaman, P. L. Vidale, A. G. Turner, M. Demory, and A. Cobb, 2017: Contribution of tropical cyclones to atmospheric moisture transport and rainfall over East Asia. *J. Climate*, **30**, 3853–3865, https://doi.org/10.1175/JCLI-D-16-0308.1.

Gutjahr, O., D. Putrasahan, K. Lohmann, J. H. Jungclaus, J.-S. von Storch, N. Brüggemann, H. Haak, and A. Stössel, 2019: Max Planck Institute Earth System Model (MPI-ESM1.2) for the High-Resolution Model Intercomparison Project (HighResMIP). *Geosci. Model Dev.*, **12**, 3241–3281, https://doi.org/10.5194/gmd-12-3241-2019.

Haarsma, R. J., and Coauthors, 2016: High Resolution Model Intercomparison Project (HighResMIP v1.0) for CMIP6. *Geosci. Model Dev.*, **9**, 4185–4208, https://doi.org/10.5194/gmd-9-4185-2016.

Hegglin, M., D. Kinnison, J.-F. Lamarque, and D. Plummer, 2016: CCMI ozone in support of CMIP6, version 1.0. Earth System Grid Federation, accessed August 2019, https://doi.org/10.22033/ESGF/input4MIPs.1115.

Hodges, K., 1995: Feature tracking on the unit sphere. *Mon. Wea. Rev.*, **123**, 3458–3465, https://doi.org/10.1175/1520-0493(1995)123<3458:FTOTUS>2.0.CO;2.

——, 1999: Adaptive constraints for feature tracking. *Mon. Wea. Rev.*, **127**, 1362–1373, https://doi.org/10.1175/1520-0493(1999)127<1362:ACFFT>2.0.CO;2.

——, A. Cobb, and P. L. Vidale, 2017: How well are tropical cyclones represented in reanalysis datasets? *J. Climate*, **30**, 5243–5264, https://doi.org/10.1175/JCLI-D-16-0557.1.

Downloaded from http://journals.ametsoc.org/jcli/article-pdf/33/7/2557/4930746/jcli190639.pdf by guest on 08 September 2020

Horn, M., and Coauthors, 2014: Tracking scheme dependence of simulated tropical cyclone response to idealized climate simulations. *J. Climate*, **27**, 9197–9213, https://doi.org/10.1175/JCLI-D-14-00200.1.

Jiang, H., and E. J. Zipser, 2010: Contribution of tropical cyclones to the global precipitation from eight seasons of TRMM data: Regional, seasonal, and interannual variations. *J. Climate*, **23**, 1526–1543, https://doi.org/10.1175/2009JCLI3303.1.

Kennedy, J., H. Titchner, N. Rayner, and M. Roberts, 2017: input4MIPs.MOHC.SSTsAndSeaIce.HighResMIP.MOHC-HadISST-2-2-0-0-0, version 20170505. Earth System Grid Federation, accessed 5 May 2017, https://doi.org/10.22033/ESGF/input4MIPs.1221.

Kim, D., and Coauthors, 2018: Process-oriented diagnosis of tropical cyclones in high-resolution GCMs. *J. Climate*, **31**, 1685–1702, https://doi.org/10.1175/JCLI-D-17-0269.1.

Klaver, R., R. Haarsma, P. L. Vidale, and W. Hazeleger, 2019: Effective resolution in high resolution global atmospheric models for climate studies. Geophysical Research Abstracts, Vol. 21, Abstract 18772, https://meetingorganizer.copernicus.org/EGU2019/EGU2019-18772-1.pdf.

Knapp, K. R., M. C. Kruk, D. H. Levinson, H. J. Diamond, and C. J. Neumann, 2010: The International Best Track Archive for Climate Stewardship (IBTrACS). *Bull. Amer. Meteor. Soc.*, **91**, 363–376, https://doi.org/10.1175/2009BAMS2755.1.

Kobayashi, S., and Coauthors, 2015: The JRA-55 Reanalysis: General specifications and basic characteristics. *J. Meteor. Soc. Japan*, **93**, 5–48, https://doi.org/10.2151/jmsj.2015-001.

Kodama, C., and Coauthors, 2015: A 20-year climatology of a NICAM AMIP-type simulation. *J. Meteor. Soc. Japan*, **93**, 393–424, https://doi.org/10.2151/jmsj.2015-024.

Kossin, J. P., K. A. Emanuel, and G. A. Vecchi, 2014: The poleward migration of the location of tropical cyclone maximum intensity. *Nature*, **509**, 349–352, https://doi.org/10.1038/nature13278.

Landsea, C. W., 2000: El Niño/Southern Oscillation and the seasonal predictability of tropical cyclones. *El Niño and the Southern Oscillation: Multiscale Variability and Global and Regional Impacts*, H. F. Diaz and V. Markgraf, Eds., Cambridge University Press, 149–182, https://doi.org/10.1017/CBO9780511573125.006.

——, and J. L. Franklin, 2013: Atlantic hurricane database uncertainty and presentation of a new database format. *Mon. Wea. Rev.*, **141**, 3576–3592, https://doi.org/10.1175/MWR-D-12-00254.1.

——, G. A. Vecchi, L. Bengtsson, and T. R. Knutson, 2010: Impact of duration thresholds on Atlantic tropical cyclone counts. *J. Climate*, **23**, 2508–2519, https://doi.org/10.1175/2009JCLI3034.1.

Lopez, P., 2002: Implementation and validation of a new prognostic large-scale cloud and precipitation scheme for climate and data-assimilation purposes. *Quart. J. Roy. Meteor. Soc.*, **128**, 229–257, https://doi.org/10.1256/00359000260498879.

MacLachlan, C., and Coauthors, 2015: Global Seasonal forecast system version 5 (GloSea5): A high-resolution seasonal forecast system. *Quart. J. Roy. Meteor. Soc.*, **141**, 1072–1084, https://doi.org/10.1002/QJ.2396.

Manganello, J. V., and Coauthors, 2012: Tropical cyclone climatology in a 10-km global atmospheric GCM: Toward weather-resolving climate modeling. *J. Climate*, **25**, 3867–3893, https://doi.org/10.1175/JCLI-D-11-00346.1.

Masson, V., and Coauthors, 2013: The SURFEXv7.2 land and ocean surface platform for coupled or offline simulation of Earth surface variables and fluxes. *Geosci. Model Dev.*, **6**, 929–960, https://doi.org/10.5194/gmd-6-929-2013.

Matthes, K., B. Funke, T. Kruschke, and S. Wahl, 2017: input4MIPs.SOLARIS-HEPPA.solar.CMIP.SOLARIS-HEPPA-3-2. Earth System Grid Federation, accessed August 2019, https://doi.org/10.22033/ESGF/input4MIPs.1122.

McTaggart-Cowan, R., T. J. Galarneau, L. F. Bosart, R. W. Moore, and O. Martius, 2013: A global climatology of baroclinically influenced tropical cyclogenesis. *Mon. Wea. Rev.*, **141**, 1963–1989, https://doi.org/10.1175/MWR-D-12-00186.1.

Mei, W., Y. Kamae, S. Xie, and K. Yoshida, 2019: Variability and predictability of North Atlantic hurricane frequency in a large ensemble of high-resolution atmospheric simulations. *J. Climate*, **32**, 3153–3167, https://doi.org/10.1175/JCLI-D-18-0554.1.

Meinshausen, M., and E. Vogel, 2016: input4MIPs.UoM.GHGConcentrations.CMIP.UoM-CMIP-1-2-0. Earth System Grid Federation, accessed August 2019, https://doi.org/10.22033/ESGF/input4MIPs.1118.

Murakami, H., 2014: Tropical cyclones in reanalysis data sets. *Geophys. Res. Lett.*, **41**, 2133–2141, https://doi.org/10.1002/2014GL059519.

——, R. Mizuta, and E. Shindo, 2012: Future changes in tropical cyclone activity project by multi-physics and multi-SST ensemble experiments using 60-km-mesh MRI-AGCM. *Climate Dyn.*, **39**, 2569–2584, https://doi.org/10.1007/s00382-011-1223-x.

——, P. Hsu, O. Arakawa, and T. Li, 2014: Influence of model biases on projected future changes in tropical cyclone frequency of occurrence. *J. Climate*, **27**, 2159–2181, https://doi.org/10.1175/JCLI-D-13-00436.1.

——, and Coauthors, 2015: Simulation and prediction of category 4 and 5 hurricanes in the high-resolution GFDL HiFLOR coupled climate model. *J. Climate*, **28**, 9058–9079, https://doi.org/10.1175/JCLI-D-15-0216.1.

Nakamura, J., and Coauthors, 2017: Western North Pacific tropical cyclone model tracks in present and future climates. *J. Geophys. Res. Atmos.*, **122**, 9721–9744, https://doi.org/10.1002/2017JD027007.

Neale, R. B., and Coauthors, 2010: Description of the NCAR Community Atmosphere Model (CAM4.0). NCAR Tech. Note NCAR/TN-485+STR, 212 pp., www.cesm.ucar.edu/models/ccsm4.0/cam/docs/description/cam4_desc.pdf.

Neu, U., and Coauthors, 2013: IMILAST: A community effort to intercompare extratropical cyclone detection and tracking algorithms. *Bull. Amer. Meteor. Soc.*, **94**, 529–547, https://doi.org/10.1175/BAMS-D-11-00154.1.

Palmer, T. N., R. Buizza, F. J. Doblas-Reyes, T. Jung, M. Leutbecher, G. Shutts, M. Steinheimer, and A. Weisheimer, 2009: Stochastic parametrization and model uncertainty. ECMWF Tech. Memo. 598, 44 pp., http://www.ecmwf.int/sites/default/files/elibrary/2009/11577-stochastic-parametrization-and-model-uncertainty.pdf.

Patricola, C. M., R. Saravanan, and P. Chang, 2018: The response of Atlantic tropical cyclones to suppression of African easterly waves. *Geophys. Res. Lett.*, **45**, 471–479, https://doi.org/10.1002/2017GL076081.

Piriou, J.-M., J.-L. Redelsperger, J.-F. Geleyn, J.-P. Lafore, and F. Guichard, 2007: An approach for convective parameterization with memory: Separating microphysics and transport in grid-scale equations. *J. Atmos. Sci.*, **64**, 4127–4139, https://doi.org/10.1175/2007JAS2144.1.

Poli, P., and Coauthors, 2016: ERA-20C: An atmospheric reanalysis of the twentieth century. *J. Climate*, **29**, 4083–4097, https://doi.org/10.1175/JCLI-D-15-0556.1.

Reed, K. A., J. T. Bacmeister, J. J. A. Huff, X. Wu, S. C. Bates, and N. A. Rosenbloom, 2019: Exploring the impact of dust on North Atlantic hurricanes in a high-resolution climate model.

Downloaded from http://journals.ametsoc.org/jcli/article-pdf/33/7/2557/4930746/jcli190639.pdf by guest on 08 September 2020

Geophys. Res. Lett., **46**, 1105–1112, https://doi.org/10.1029/2018GL080642.

Ren, F., J. Liang, G. Wu, W. Dong, and X. Yang, 2011: Reliability analysis of climate change of tropical cyclone activity over the western North Pacific. *J. Climate*, **24**, 5887–5898, https://doi.org/10.1175/2011JCLI3996.1.

Roberts, C. D., R. Senan, F. Molteni, S. Boussetta, S. Keeley, 2017a: ECMWF ECMWF-IFS-LR model output prepared for CMIP6 HighResMIP, version 20170915. Earth System Grid Federation, accessed August 2019, https://doi.org/10.22033/ESGF/CMIP6.2463.

——, ——, ——, ——, and ——, 2017b: ECMWF ECMWF-IFS-HR model output prepared for CMIP6 HighResMIP, version 20170915. Earth System Grid Federation, accessed August 2019, https://doi.org/10.22033/ESGF/CMIP6.2461.

——, ——, ——, ——, M. Mayer, and S. Keeley, 2018: Climate model configurations of the ECMWF Integrated Forecast System (ECMWF-IFS cycle 43r1) for HighResMIP. *Geosci. Model Dev.*, **11**, 3681–3712, https://doi.org/10.5194/gmd-11-3681-2018.

Roberts, M., 2017a: MOHC HadGEM3-GC31-LM model output prepared for CMIP6 HighResMIP, version 20170906. Earth System Grid Federation, accessed August 2019, https://doi.org/10.22033/ESGF/CMIP6.1321.

——, 2017b: MOHC HadGEM3-GC31-MM model output prepared for CMIP6 HighResMIP, version 20180818. Earth System Grid Federation, accessed August 2019, https://doi.org/10.22033/ESGF/CMIP6.1902.

——, 2017c: MOHC HadGEM3-GC31-HM model output prepared for CMIP6 HighResMIP, version 20170831. Earth System Grid Federation, accessed August 2019, https://doi.org/10.22033/ESGF/CMIP6.446.

——, 2019a: CMIP6 HighResMIP: Tropical storm tracks as calculated by the TRACK algorithm. Centre for Environmental Data Analysis, accessed August 2019, http://catalogue.ceda.ac.uk/uuid/0b42715a7a804290afa9b7e31f5d7753.

——, 2019b: CMIP6 HighResMIP: Tropical storm tracks as calculated by the TempestExtremes algorithm. Centre for Environmental Data Analysis, accessed August 2019, http://catalogue.ceda.ac.uk/uuid/438268b75fed4f27988dc02f8a1d756d.

——, and Coauthors, 2013: Sensitivity of tropical cyclone simulation to SST forcing. *U.S. CLIVAR Variations*, Vol. 11, No. 3, U.S. CLIVAR Project Office, Washington, DC, 12–17, https://usclivar.org/sites/default/files/USCLIVAR_VARIATIONS_11_3_Fall2013.pdf.

——, and Coauthors, 2015: Tropical cyclones in the UPSCALE ensemble of high-resolution global climate models. *J. Climate*, **28**, 574–596, https://doi.org/10.1175/JCLI-D-14-00131.1.

——, and Coauthors, 2019: Description of the resolution hierarchy of the global coupled HadGEM3-GC3.1 model as used in CMIP6 HighResMIP experiments. *Geosci. Model Dev.*, **12**, 4999–5028, https://doi.org/10.5194/gmd-12-4999-2019.

Saha, S., and Coauthors, 2014: The NCEP Climate Forecast System version 2. *J. Climate*, **27**, 2185–2208, https://doi.org/10.1175/JCLI-D-12-00823.1.

Sanchez, C., K. D. Williams, and M. Collins, 2016: Improved stochastic physics schemes for global weather and climate models. *Quart. J. Roy. Meteor. Soc.*, **142**, 147–159, https://doi.org/10.1002/qj.2640.

Scaife, A. A., and Coauthors, 2019: Does increased atmospheric resolution improve seasonal climate predictions? *Atmos. Sci. Lett.*, **20**, e922, https://doi.org/10.1002/asl.922.

Scoccimarro, E., S. Gualdi, G. Villarini, G. A. Vecchi, M. Zhao, K. Walsh, and A. Navarra, 2014: Intense precipitation events associated with landfalling tropical cyclones in response to a warmer climate and increased CO_2. *J. Climate*, **27**, 4642–4654, https://doi.org/10.1175/JCLI-D-14-00065.1.

——, A. Bellucci, D. Peano, 2017a: CMCC CMCC-CM2-HR4 model output prepared for CMIP6 HighResMIP hist-1950. Earth System Grid Federation, accessed August 2019, https://doi.org/10.22033/ESGF/CMIP6.1359.

——, ——, and ——, 2017b: CMCC CMCC-CM2-VHR4 model output prepared for CMIP6 HighResMIP. Earth System Grid Federation, accessed August 2019, https://doi.org/10.22033/ESGF/CMIP6.1367.

——, P. G. Fogli, K. Reed, S. Gualdi, S. Masina, and A. Navarra, 2017c: Tropical cyclone interaction with the ocean: The role of high-frequency (subdaily) coupled processes. *J. Climate*, **30**, 145–162, https://doi.org/10.1175/JCLI-D-16-0292.1.

——, A. Bellucci, A. Storto, S. Gualdi, S. Masina, and A. Navarra, 2018: Remote sub-surface ocean temperature as a predictor of Atlantic hurricane activity. *Proc. Natl. Acad. Sci. USA*, **115**, 11 460–11 464, https://doi.org/10.1073/pnas.1810755115.

——, S. Gualdi, A. Bellucci, D. Peano, A. Cherchi, and A. Navarra, 2020: The typhoon-induced drying of the Maritime Continent. *Proc. Natl. Acad. Sci. USA*, https://doi.org/10.1073/pnas.1915364117, in press.

Shaevitz, D. A., and Coauthors, 2014: Characteristics of tropical cyclones in high-resolution models in the present climate. *J. Adv. Model. Earth Syst.*, **6**, 1154–1172, https://doi.org/10.1002/2014MS000372.

Shields, C. A., and Coauthors, 2018: Atmospheric River Tracking Method Intercomparison Project (ARTMIP): Project goals and experimental design. *Geosci. Model Dev.*, **11**, 2455–2474, https://doi.org/10.5194/gmd-11-2455-2018.

Stevens, B., S. Fiedler, S. Kinne, K. Peters, S. Rast, J. Müsse, S. J. Smith, and T. Mauritsen, 2017: MACv2-SP: A parameterization of anthropogenic aerosol optical properties and an associated Twomey effect for use in CMIP6. *Geosci. Model Dev.*, **10**, 433–452, https://doi.org/10.5194/gmd-10-433-2017.

Strachan, J., P. L. Vidale, K. Hodges, M. Roberts, and M. E. Demory, 2013: Investigating global tropical cyclone activity with a hierarchy of AGCMs: The role of model resolution. *J. Climate*, **26**, 133–152, https://doi.org/10.1175/JCLI-D-12-00012.1.

Sun, Y., and Coauthors, 2017: Impact of ocean warming on tropical cyclone track over the western North Pacific: A numerical investigation based on two case studies. *J. Geophys. Res. Atmos.*, **122**, 8617–8630, https://doi.org/10.1002/2017JD026959.

Tang, B., and S. J. Camargo, 2014: Environmental control of tropical cyclones in CMIP5: A ventilation perspective. *J. Adv. Model. Earth Syst.*, **6**, 115–128, https://doi.org/10.1002/2013MS000294.

Taylor, K. E., D. Williamson, and F. Zwiers, 2000: The sea surface temperature and sea ice concentration boundary conditions for AMIP II simulations. Lawrence Livermore National Laboratory Program for Climate Model Diagnosis and Intercomparison Rep. 60, 28 pp., https://pcmdi.llnl.gov/report/ab60.html.

Thorncroft, C., and K. Hodges, 2001: African easterly wave variability and its relationship to Atlantic tropical cyclone activity. *J. Climate*, **14**, 1166–1179, https://doi.org/10.1175/1520-0442(2001)014<1166:AEWVAI>2.0.CO;2.

Ullrich, P. A., and C. M. Zarzycki, 2017: TempestExtremes: A framework for scale-insensitive pointwise feature tracking on unstructured grids. *Geosci. Model Dev.*, **10**, 1069–1090, https://doi.org/10.5194/gmd-10-1069-2017.

Vecchi, G. A., and Coauthors, 2019: Tropical cyclone sensitivities to CO_2 doubling: Roles of atmospheric resolution, synoptic

Downloaded from http://journals.ametsoc.org/jcli/article-pdf/33/7/2557/4930746/jcli190639.pdf by guest on 08 September 2020

variability and background climate changes. *Climate Dyn.*, **53**, 5999–6033, https://doi.org/10.1007/s00382-019-04913-y.

Villarini, G., and G. A. Vecchi, 2013: Multiseason lead forecast of the North Atlantic power dissipation index (PDI) and accumulated cyclone energy (ACE). *J. Climate*, **26**, 3631–3643, https://doi.org/10.1175/JCLI-D-12-00448.1.

Voldoire, A., 2017: CNRM-CERFACS CNRM-CM6-1-HR model output prepared for CMIP6 HighResMIP. Earth System Grid Federation, accessed August 2019, https://doi.org/10.22033/ESGF/CMIP6.1387.

——, 2018: CNRM-CERFACS CNRM-CM6-1 model output prepared for CMIP6 HighResMIP. Earth System Grid Federation, accessed August 2019, https://doi.org/10.22033/ESGF/CMIP6.1925.

——, and Coauthors, 2013: The CNRM-CM5.1 global climate model: Description and basic evaluation. *Climate Dyn.*, **40**, 2091–2121, https://doi.org/10.1007/s00382-011-1259-y.

——, and Coauthors, 2019: Evaluation of CMIP6 DECK experiments with CNRM-CM6-1. *J. Adv. Model. Earth Syst.*, **11**, 2177–2213, https://doi.org/10.1029/2019MS001683.

von Storch, J.-S., and Coauthors, 2017a: MPI-M MPI-ESM1.2-HR model output prepared for CMIP6 HighResMIP. Earth System Grid Federation, accessed August 2019, https://doi.org/10.22033/ESGF/CMIP6.762.

——, and Coauthors, 2017b: MPI-M MPI-ESM1.2-XR model output prepared for CMIP6 HighResMIP. Earth System Grid Federation, accessed August 2019, https://doi.org/10.22033/ESGF/CMIP6.10290.

Walsh, K., S. Lavender, H. Murakami, E. Scoccimarro, L.-P. Caron, and M. Ghantous, 2010: The Tropical Cyclone Climate Model Intercomparison Project. *Hurricanes and Climate Change*, Vol. 2, J. Elsner et al., Eds., Springer, 1–24.

——, ——, E. Scoccimarro, and H. Murakami, 2013: Resolution dependence of tropical cyclone formation in CMIP3 and finer resolution models. *Climate Dyn.*, **40**, 585–599, https://doi.org/10.1007/s00382-012-1298-z.

——, and Coauthors, 2015: Hurricanes and climate: The U.S. CLIVAR working group on hurricanes. *Bull. Amer. Meteor. Soc.*, **96**, 997–1017, https://doi.org/10.1175/BAMS-D-13-00242.1.

——, and Coauthors, 2016: Tropical cyclones and climate change. *Wiley Interdiscip. Rev.: Climate Change*, **7**, 65–89, https://doi.org/10.1002/wcc.371.

Walters, D., and Coauthors, 2019: The Met Office Unified Model Global Atmosphere 7.0/7.1 and JULES Global Land 7.0 configurations. *Geosci. Model Dev.*, **12**, 1909–1963, https://doi.org/10.5194/gmd-12-1909-2019.

Watson, P. A. G., J. Berner, S. Corti, P. Davini, J. von Hardenberg, C. Sanchez, A. Weisheimer, and T. N. Palmer, 2017: The impact of stochastic physics on tropical rainfall variability in global climate models on daily to weekly time scales. *J. Geophys. Res. Atmos.*, **122**, 5738–5762, https://doi.org/10.1002/2016JD026386.

Wehner, M. F., and Coauthors, 2014: The effect of horizontal resolution on simulation quality in the Community Atmospheric Model, CAM5.1. *J. Adv. Model. Earth Syst.*, **6**, 980–997, https://doi.org/10.1002/2013MS000276.

Williams, K. D., and Coauthors, 2015: The Met Office Global Coupled model 2.0 (GC2) configuration. *Geosci. Model Dev.*, **8**, 1509–1524, https://doi.org/10.5194/gmd-8-1509-2015.

——, and Coauthors, 2017: The Met Office Global Coupled model 3.0 and 3.1 (GC3.0 and GC3.1) configurations. *J. Adv. Model. Earth Syst.*, **10**, 357–380, https://doi.org/10.1002/2017MS001115.

Wood, N., and Coauthors, 2014: An inherently mass-conserving semi-implicit semi-Lagrangian discretization of the deep-atmosphere global non-hydrostatic equations. *Quart. J. Roy. Meteor. Soc.*, **140**, 1505–1520, https://doi.org/10.1002/qj.2235.

Yanase, W., H. Niino, K. Hodges, and N. Kitabatake, 2014: Parameter spaces of environmental fields responsible for cyclone development from tropics to extratropics. *J. Climate*, **27**, 652–671, https://doi.org/10.1175/JCLI-D-13-00153.1.

Yoshida, K., M. Sugi, R. Mizuta, H. Murakami, and M. Ishii, 2017: Future changes in tropical cyclone activity in high-resolution large-ensemble simulations. *Geophys. Res. Lett.*, **44**, 9910–9917, https://doi.org/10.1002/2017GL075058.

Zarzycki, C. M., 2016: Tropical cyclone intensity errors associated with lack of two-way ocean coupling in high-resolution global simulations. *J. Climate*, **29**, 8589–8610, https://doi.org/10.1175/JCLI-D-16-0273.1.

——, and P. A. Ullrich, 2017: Assessing sensitivities in algorithmic detection of tropical cyclones in climate data. *Geophys. Res. Lett.*, **44**, 1141–1149, https://doi.org/10.1002/2016GL071606.

Zhao, M., and I. M. Held, 2012: TC-permitting GCM simulations of hurricane frequency response to sea surface temperature anomalies projected for the late-twenty-first century. *J. Climate*, **25**, 2995–3009, https://doi.org/10.1175/JCLI-D-11-00313.1.

——, ——, S. Lin, and G. A. Vecchi, 2009: Simulations of global hurricane climatology, interannual variability, and response to global warming using a 50-km resolution GCM. *J. Climate*, **22**, 6653–6678, https://doi.org/10.1175/2009JCLI3049.1.

Downloaded from http://journals.ametsoc.org/jcli/article-pdf/33/7/2557/4930746/jcli190639.pdf by guest on 08 September 2020